



1
2
3
4
5
6
7
8
9
10
11
12
13
14
15
16
17
18
19
20
21
22
23
24
25
26
27
28
29
30
31

Water Resources Research

Stable and Radioisotope Systematics Reveal Fossil Water as Fundamental Characteristic of Arid Orogenic-Scale Groundwater Systems

Brendan J. Moran (ORCID = 0000-0002-9862-6241)¹, David F. Boutt (ORCID = 0000-0003-1397-0279)¹, Lee Ann Munk (ORCID =0000-0003-2850-545X)²

¹ Department of Geosciences, University of Massachusetts-Amherst, Amherst, MA, USA

² Department of Geological Sciences, 3101 Science Circle, University of Alaska-Anchorage, Anchorage, AK, USA

Corresponding author: Brendan J. Moran (bmoran@geo.umass.edu)

Key points

- Analysis of tritium in water discharging within Salar de Atacama basin show it is composed predominantly of water >60 years old.
- Water entering the Salar de Atacama basin is spatially distinct and decoupled from recharge on the Altiplano-Puna plateau.
- Analysis of stable O and H isotope ratios in 900 water samples constrain the spatiotemporal dimensions of modern and fossil groundwaters.

Keywords: Salar de Atacama, Chile; paleo-recharge; Tritium; Altiplano-Puna plateau; regional groundwater flow

32 **Abstract**

33 In arid and semi-arid regions, persistent hydrological imbalances illuminate the
34 considerable gaps in our spatiotemporal understanding of fundamental catchment-scale governing
35 mechanisms. The Salar de Atacama basin is the most extreme example of groundwater-
36 dominated continental basins and therefore is an ideal place to probe these unresolved questions.
37 Geochemical and hydrophysical observations indicate that groundwaters discharging into the
38 basin reflect a large regional system integrated over 10^2 - 10^4 year time-scales. The groundwater
39 here, as in other arid regions is a critical freshwater resource subject to substantial demand from
40 competing interests, particularly as development of its world-class lithium brine deposit expands.
41 Utilizing a uniquely large and comprehensive set of H and O isotopes in water we demonstrate
42 that much of the presumed recharge area on the Altiplano-Puna plateau exhibits isotopic
43 signatures quite distinct from waters presently discharging within the endorheic Salar de Atacama
44 watershed. $\delta^{18}\text{O}$ values of predicted inflow source waters are 3.6‰ to 5.6‰ higher than modern
45 plateau waters and ^3H data from 87 discrete samples indicate nearly all of this inflow is composed
46 of pre-modern recharge (i.e. fossil water). Under plausible conditions, these distinctions cannot
47 be explained solely by natural variability in modern meteoric inputs or by steady-state
48 groundwater flow. We present a conceptual model revealing the extensive influence of transient
49 draining of fossil groundwater storage augmented by regional interbasin flow from the Andes.
50 Our analysis provides robust constraints on fundamental mechanisms governing this arid
51 continental groundwater system and a framework within which to address persistent uncertainties
52 in similar systems worldwide.

53 **Plain Language Summary**

54 Groundwater in the driest places on Earth is a vital resource for both humans and
55 ecosystems, yet fundamental characteristics of this water such as where it originates and how it
56 moves in the ground remain unresolved. This water often lies deep underground and flows across
57 great distances and over long periods of time, as a result, it is quite difficult to study. Using the
58 1000 water samples in the Salar de Atacama basin in northern Chile at the border of the driest
59 desert on Earth we trace the origin and travel time of water across a large region. Groundwater in
60 the Salar de Atacama region is fundamental to sustaining natural and human systems, therefore,
61 developing a better understanding of how this water moves will be critical for their management,
62 particularly as development of its world-class lithium brine deposit expands. We find that ‘fossil
63 water’ which entered the ground hundreds or thousands of years ago makes up most of the water
64 now flowing into the basin. Our analysis also defines the area which contributes water to the
65 basin, much of which incorporates flow through mountains and from other higher elevation

66 basins. By improving our understanding of how these large flow systems develop and function
67 this work will aid efforts to sustainably manage these critical freshwater resources for all who
68 rely on them.

69

70 **1. Introduction**

71 In the driest places on Earth, internally drained basins of various scales exhibit
72 groundwater discharge rates that exceed modern recharge (Gleeson et al., 2012; Scanlon et al.,
73 2006; Van Beek et al., 2011). These hydrologic budget imbalances have been observed or
74 inferred in nearly every arid region including: the southwestern United States (Belcher et al.,
75 2009; Kafri et al., 2012, Love et al., 2018; Wheatler et al., 2007), the Himalayan-Tibetan plateau
76 (Ge et al., 2016 and references therein), central Australia (Skrzypek et al., 2016; Wood et al.,
77 2015), the Sahara desert (Gasse et al., 2000; Kröpelin et al., 2008), the Arabian peninsula (Burg et
78 al. 2013; Müller et al., 2016; Wheatler et al., 2007) and the central Andes (Corenthal et al., 2016
79 and references therein). Difficulty constraining fundamental hydrological processes such as
80 response times, flow paths and distribution and timing of groundwater recharge is magnified by
81 long residence times (>1 ka), deep water tables (>100 m) and often insufficient data (Favreau et
82 al., 2009; Gleeson et al., 2011; Walvoord et al., 2002). Uncertainties among inputs are
83 compounded by equally large uncertainties in discharge, which in these endorheic systems occurs
84 exclusively through evapotranspiration (Kampf & Tyler, 2006; Tyler et al., 1997). Fundamental
85 uncertainties have perpetuated inconsistencies in our conceptual models of system-wide
86 groundwater flow and the spatiotemporal dimensions of this flow, as a result, it is clear that
87 current conceptual models need to be adjusted or altogether re-evaluated (e.g. Currell et al., 2016;
88 Haitjema & Mitchell-Bruker, 2005).

89 In the Preandean Depression, a large intramontane depression on the margin of the hyper-
90 arid core of the Atacama Desert and the Central Andean Plateau, it has been shown that water and
91 solute budgets are difficult to close under currently accepted catchment dimensions (Figure 1). In
92 the Río Loa watershed to the north (i.e. Calama Basin), anomalous water discharge volumes have
93 been observed (e.g., Jordan et al., 2015) and the Central Depression to the west has anomalous
94 nitrate accumulation (Pérez-Fodich et al., 2014). The most prominent feature in the region, the
95 Salar de Atacama basin is defined by very large elevation and precipitation gradients which have
96 led to the development of an orogenic-scale groundwater system encompassing portions of the
97 adjacent Altiplano-Puna plateau. Recent work has concluded that solute and water influxes to
98 Salar de Atacama would need to be 9-20 times greater than modern to account for the massive

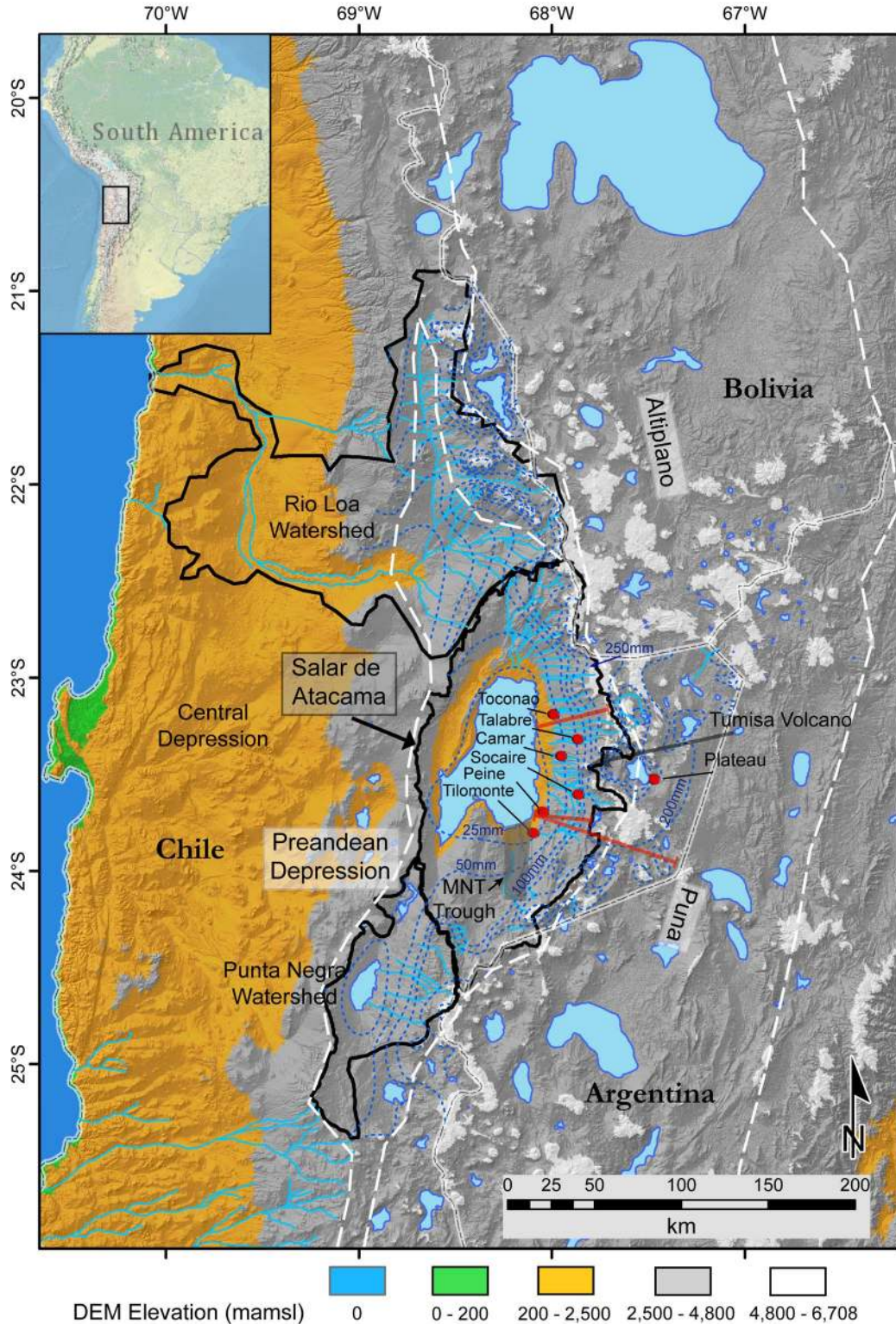


Figure 1. Digital elevation map of the Central Andes. Salars, lagoons and major drainages (quebradas and rivers) are light blue. Topographic watersheds of major basins are outlined in black. Extent of the Preandean Depression and Altiplano-Puna plateau are outlined in white dashes. Isohyetal contours in mm/year are dark blue dashed lines. Locations of generalized geologic cross-sections in Figure S1 are red. Red dots are precipitation gauges and sites used for HYSPLIT models. MNT Trough structure is shaded.

100 evaporite deposit accumulated there since the Miocene (Boutt et al., 2018; Corenthal et al., 2016),
101 but also that it is possible to accumulate the Li deposit from low-temperature weathering within a
102 reasonable timeframe (Munk et al., 2018). Fundamental aspects of subsurface fluid flow remain
103 unresolved including (i) catchment-wide response times to changes in recharge and water tables,
104 (ii) spatial and temporal connections between the modern and paleo-hydrological systems, and
105 (iii) the sources of additional water and solutes required to balance mass at various scales. The
106 Salar de Atacama basin and its larger groundwater system is an ideal place to methodically
107 address these questions; this work advances our understanding of each.

108 The hydrogeologic system of Salar de Atacama ranks as the most extreme on Earth; on
109 the margin of the driest non-polar desert and flanked by one of the highest and broadest plateaus
110 (Hartley & Chong, 2002). These extreme conditions, persistent for at least 7 Ma, longer than any
111 other place on the planet (Jordan et al., 2002; Rech et al., 2019) have produced its hydrological
112 characteristics. The near total lack of vegetation and surface water other than where groundwater
113 meets the surface, coupled with large precipitation and topographic gradients allow for
114 identification and delineation of distinct groundwater systematics. Accordingly, large-scale
115 governing mechanisms are also magnified and easily characterized and constrained. The
116 combined effect of these characteristics allows fundamental properties of the system to be
117 accurately interpreted within an integrated region-wide analysis.

118 We utilize a novel and comprehensive dataset of ~1000 individual water samples
119 covering approximately 28000 km² to identify ‘fossil water’ (defined herein as water which
120 entered the ground prior to 60 years ago) currently manifest in this system and define how it
121 interacts with the modern hydrologic regime. Analysis of oxygen (¹⁸O/¹⁶O) and hydrogen (²H/¹H)
122 isotope ratios show inflows within the basin from springs and diffuse groundwaters have a
123 consistently higher $\delta^{18}\text{O}$ and $\delta^2\text{H}$ signatures relative to presumed source waters revealing
124 important distinctions among inflow and recharge waters. Tritium (³H) content in 87 discrete
125 inflow waters are almost entirely ³H-dead, defining a pronounced disconnect between modern
126 inputs and groundwater region-wide. These results coupled with hydrophysical, geological and
127 atmospheric data suggest that large portions of the adjacent plateau are not hydraulically
128 connected to shallow groundwaters presently discharging into the Salar de Atacama basin and
129 modern (<60 years), local meteoric inputs to the system are limited. We present an integrated
130 conceptual model demonstrating that steady-state assumptions are inadequate, watershed
131 boundaries must be redefined and transient head-decay of groundwater storage over thousand-
132 year time scales is a critical component of the present hydrogeologic system.

133 **2. Hydrogeologic Setting**

134 Endorheic basins are topographically closed with a negative annual water balance, these
 135 systems often develop salars (salt pans) at their floors (Eugster, 1980; Rosen, 1994). Local flow
 136 paths mimic topography and occur between adjacent higher and lower elevation zones, while
 137 regional flow paths may cross topographic boundaries (Haitjema & Mitchell-Bruker, 2005; Tóth,
 138 1963). Typical of other mountainous arid regions, the Salar de Atacama basin can be divided into
 139 high elevation areas where most recharge occurs, a zone of lateral fluid flow and a discharge area
 140 near the basin floor (Maxey, 1968). High vertical relief and precipitation gradients have
 141 contributed to the development of an extensive regional groundwater flow system.

142 The Salar de Atacama basin coincides with a sharp bend in the modern Andean volcanic
 143 arc which retreats 60 km east from its regional N-S trend (Reutter et al., 2006) (Figure 1). The
 144 salar at its floor covers 3000 km² at 2300 mamsl and is flanked by the Andean Cordillera (~5500
 145 mamsl) to the north, south, and east and by the Cordillera de Domeyko (~3500 mamsl) to the
 146 west. Its topographic watershed encompasses 17000 km², divided to the east and southeast by
 147 several high volcanic peaks (Figure 1) which form the western margin of the Altiplano-Puna
 148 plateau, a broad expanse of volcanic peaks and basins between 4000 mamsl and 6000 mamsl
 149 (Allmendinger et al., 1997; Jordan et al., 2010). It consists of a succession of volcanic units
 150 deposited during the last 10 Ma by large caldera-forming eruptions, small volume mafic centers
 151 and numerous stratovolcanoes (Strecker et al., 2007; Ward et al., 2014). These volcanoclastic
 152 deposits have relatively high permeability (Gardeweg & Ramirez, 1987; WMC, 2007).

153 Numerous Miocene ignimbrites draped across the region and alluvial fans along the
 154 flanks of the Salar de Atacama basin are important controls on springs and diffuse inflows at the
 155 margin of the basin floor (Jordan et al., 2002; Mather & Hartley, 2005) (Figure S1). The
 156 fractured unwelded and moderately welded ignimbrites exhibit high infiltration capacity and
 157 permeability providing major flow paths for local and regional groundwater, while welded
 158 ignimbrites may act as confining units (Herrera et al., 2016; Houston, 2009). Large clastic
 159 deposits, many of Miocene age and buried alluvial fans such as those near the topographic divide
 160 and along the salar margins provide substantial storage capacity and are conduits for deep
 161 groundwater transport within the eastern slopes of the basin (Houston, 2009; Wilson & Guan,
 162 2004) (Figure S1).

163 The eastern margin of the basin contains several sub-watersheds delineated by a 60 km
 164 long N–S oriented trough in the south called the Monturaqui–Negrillar–Tilopozo (MNT); the
 165 Miscanti fault and fold system to the east separates the basin from the Andes and controls the

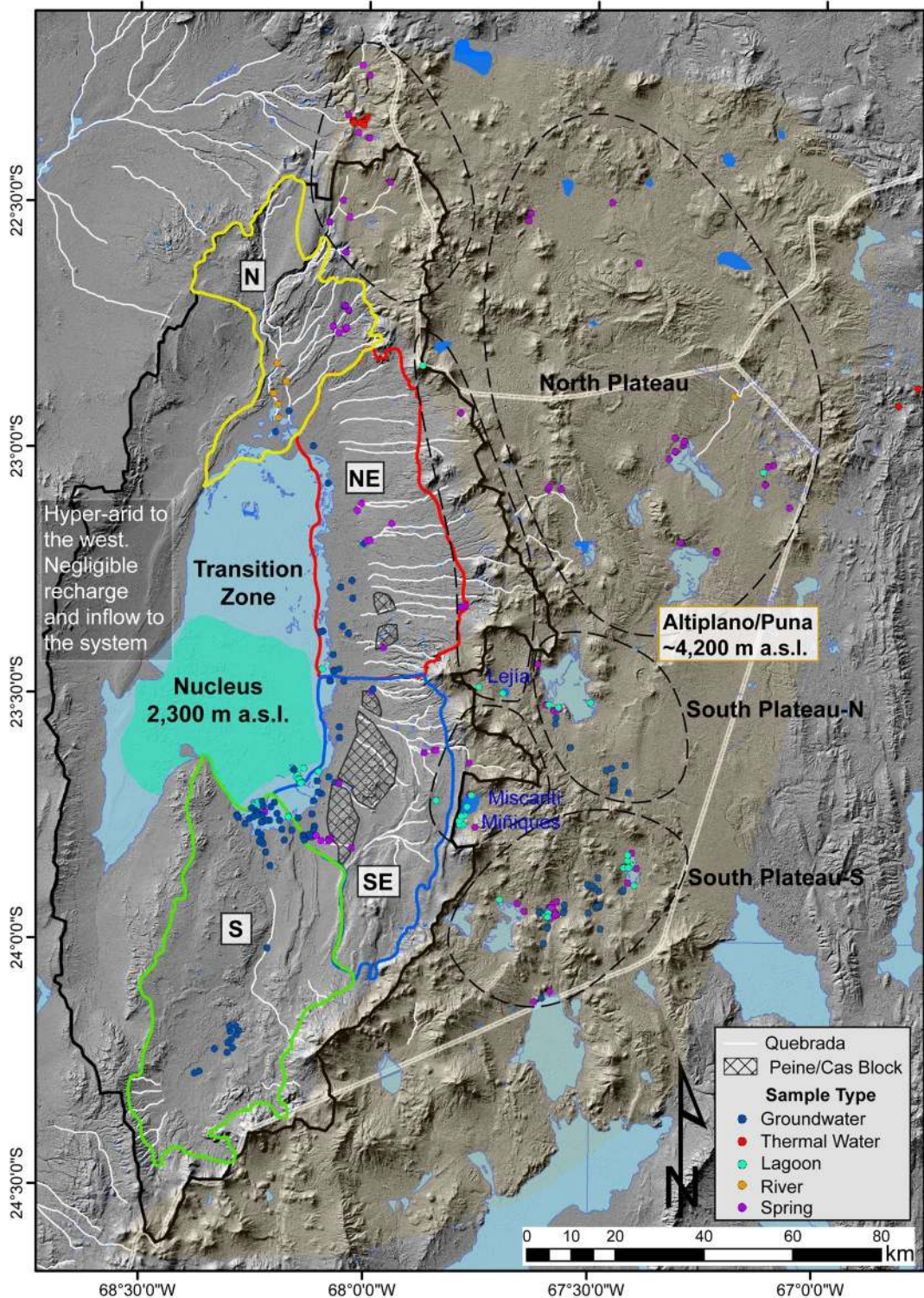


Figure 2. The Salar de Atacama topographic watershed (solid black line), its recharge zones (black dashed ellipses) and discharge/inflow zones (solid colored lines). Dots represent sample sites, grouped by water type. Discharge zones extend from the salar margin to 4000 mamsl. Major drainages (quebradas and rivers) are shown in white and salars and lagoons in light blue and dark blue respectively. Notable high elevation lagoons Miñiques, Miscanti and Lejía are labeled. Surface expression of the Peine/Cas structure is hatched.

167 development of the intra-arc lakes Miñiques and Miscanti and the broad Tumisa volcano divides
168 the northeast from the southeast sub-watersheds (Aron et al., 2008; Rissmann et al., 2015) (Figure
169 1 & S1). A large Paleozoic structural block (Peine/Cas block), bounded by the N-S trending
170 Toloncha fault and fold system and Peine fault is interposed in the center of the southeastern
171 slope forming a major hydrogeologic obstruction that diverts, restricts and focuses groundwater
172 flow through this zone (Aron et al., 2008; Boutt et al., 2018; Breitreuz, 1995; Gonzalez et al.,
173 2009; Jordan et al., 2002; Ruetter et al., 2006) (Figure 2). The N-S fold and thrust belt
174 architecture of the basin slope forms several fault systems of varying extent and depth parallel to
175 the salar margin; these and associated lower-order faults are thought to be major conduits for
176 groundwater flow to the surface as evidenced by the spring complexes emerging along or in the
177 vicinity of these zones (Jordan et al., 2002).

178 The extreme aridity here is a result of subsiding air within the subtropical high-pressure
179 zone, the presence of the cold Humboldt current off the Pacific coast and the Andean Cordillera
180 acting as a high orographic barrier to precipitation from the east (Garreaud et al., 2003; Hartley &
181 Chong, 2002). Rainfall varies significantly annually but on average the majority of precipitation
182 falls during the Austral summer and La Niña episodes (Houston, 2006a; Magilligan et al., 2008).
183 Within the watershed and on the plateau, there are strong orographic effects on precipitation.
184 Annual precipitation at the basin floor averages only 15 mm/year while many areas over 4500
185 mamsl within the topographic watershed average about 250 mm/year (DGA, 2013; Houston,
186 2006b). Of this high-altitude precipitation, approximately 50 to 80 mm of snow water equivalent
187 falls each year above 4500 mamsl, however much of this liquid sublimates due to high insolation
188 and low relative humidity (DGA, 2013; Vuille & Ammann, 1997). There is no permanent ice at
189 present and it is likely that there was no glaciation in this portion of the Andes even at the highest
190 altitudes (Ammann, et al., 2001; Ward et al., 2015).

191 Paleoclimate records indicate that hyper-arid conditions dominated prior to 325 ka in this
192 region but that a more variable climate has existed since, especially during the most recent glacial
193 cycle (Bobst et al., 2001; Lowenstein et al., 2003). During the Central Andean Pluvial Event
194 from about 18-8 ka, altiplano lake levels increased by tens of meters (Blard et al., 2011; Blodgett
195 et al., 1997; Fritz et al., 2004; Placzek et al., 2006, 2009, 2013; Sáez et al., 2016), and a smaller
196 amplitude but substantial wet phase occurred around 4-5 ka (De Porras et al., 2017; Rech et al.,
197 2003). Sediment cores, rodent middens and paleo-wetland records indicate that during the
198 Holocene the climate was somewhat wetter until about 3 ka when it shifted to its modern regime
199 (Betancourt et al., 2000; Bobst et al., 2001; Latorre et al., 2003; Quade et al., 2008; Rech et al.,
200 2002). Laguna Lejía approximately 40 km east of the salar at 4325 mamsl at its late-glacial high

201 stage was ~25 m higher than today which would require double the modern precipitation rate, up
202 to 500 mm/year (Grosjean et al., 1995; Grosjean & Núñez, 1994).

203 **3. Methods**

204 3.1 Water Tracer Data

205 Surface and groundwater samples analyzed for this study were collected during numerous
206 field campaigns between October 2011 and December 2017. In addition, we utilized all available
207 published data and reports to supplement our dataset (Table S1). Samples were collected with a
208 consistent, standardized procedure and when possible, seasonally from the same location. All
209 samples were filtered through a 0.45-micron filter and groundwater samples were extracted from
210 wells screened at or below the water table with a peristaltic pump through clean polyethylene
211 tubing or with a clean bailer. In-situ measurements of temperature, specific conductance, and pH
212 were made at each sampling location during collection. Locations of all stable and radioisotope
213 samples are presented in Figure 2, a detailed analytical procedure for these analyses is provided in
214 supplemental material (Text S2).

215 3.2 Discharge Zones, Recharge Zones and Water Types

216 Sub-watersheds (zones of inflow) to the Salar de Atacama basin, designated N, NE, SE
217 and S were defined by topography, hydrogeology and isotopic characteristics (Figure 2). All
218 shallow (<120 mbgl) inflow entering the basin is divided into these discrete zones corresponding
219 closely to the “watershed regions” and “groundwater flux basins” defined by Munk et al. (2018).
220 Explicit boundaries at the margins of these zones were defined by groundwater contouring and
221 flow directions determined from groundwater level measurements in the field. At high elevation,
222 six groundwater recharge zones were delineated based on topography and orientation relative to
223 the Salar de Atacama watershed. Three of these zones straddle the watershed divide where
224 hydrologic conditions are distinct from the plateau further east. This facilitates a detailed
225 spatiotemporal analysis of water isotope signatures among recharge and discharge waters allows
226 for an examination of sources and flow paths and ultimately to constrain dominant hydrological
227 mechanisms within and between these zones.

228 All data were categorized into six water types (Groundwater, Spring, Spring-fed River,
229 River, Lagoon, and Thermal) designed to facilitate inter-comparison and interpretation of results.
230 Almost no vegetation exists except where freshwater bodies intersect the surface, consequently,
231 these water classifications were reliably determined with the use of satellite imagery and field

232 observations. Groundwater is herein defined as samples taken directly from wells (e.g.
233 monitoring, pumping) that are open to the aquifer at depths ranging from 1 to ~120 mbgl. Spring
234 water denotes perennially flowing groundwater discharge and Spring-fed Rivers are waters fed
235 predominantly by groundwater discharge a short distance (<1 km) upgradient of where it was
236 sampled. These waters are herein grouped with Spring waters because our analysis shows them to
237 be isotopically indistinguishable. Rivers are defined as large systems of perennially flowing
238 surface waters >10 km in length. Lagoons are surface water that is perennially extant at the
239 surface, including freshwater lakes, wetlands, and brackish-to-salt lagoons. Thermal waters are
240 from geysers or thermal pools directly influenced by geothermal heat with temperatures between
241 ~40° to ~80° C. The distinction between these water types is based on extensive knowledge of the
242 regional hydrogeology gathered during more than ten field campaigns, previous published work
243 and scrutiny of isotopic signatures.

244 3.3 Atmospheric Back-Trajectory Modelling

245 To constrain prevailing atmospheric moisture sources in the modern climate system we
246 calculated 5-day air parcel back-trajectories using NOAA Air Resources Laboratory's HYSPLIT
247 Transport and Dispersion Model for all large and extensive precipitation events in the region over
248 the past 20 years (1997-2017) (DGA, 2013; Draxler & Hess, 1998). More detail is provided in
249 supplementary material (Text S2).

250 4. Results

251 4.1 Tritium

252 Our exhaustive set of water samples from the Salar de Atacama watershed were analyzed
253 for ³H isotope content of the water molecules, these ³H values are used as a direct tracer of Mean
254 Residence Time (MRT) and source (Table S1). We determine a “percent modern water” (R_{mod})
255 in these samples not as a direct estimate of the modern water content but rather as a relative value
256 to compare connections with modern meteoric inputs. To determine R_{mod} we first constrain the
257 average ³H content of modern precipitation in the region. This value, also presented by Boutt et
258 al. (2016) was determined to be 3.23 ± 0.6 TU (1σ) from five carefully chosen rain samples
259 collected during 2013 and 2014 (locations in Figure 3). This agrees with the range of values from
260 Cortecchi et al. (2005), Grosjean et al. (1995), Herrera et al. (2016) and Houston (2002, 2007). We
261 use a value on the lower end of the published range (3.23TU) based on the assumption that
262 smaller precipitation events are unlikely to produce actual recharge in this environment and
263 events with the lowest tritium values (sourced from the Pacific Ocean) are reflective of decade-

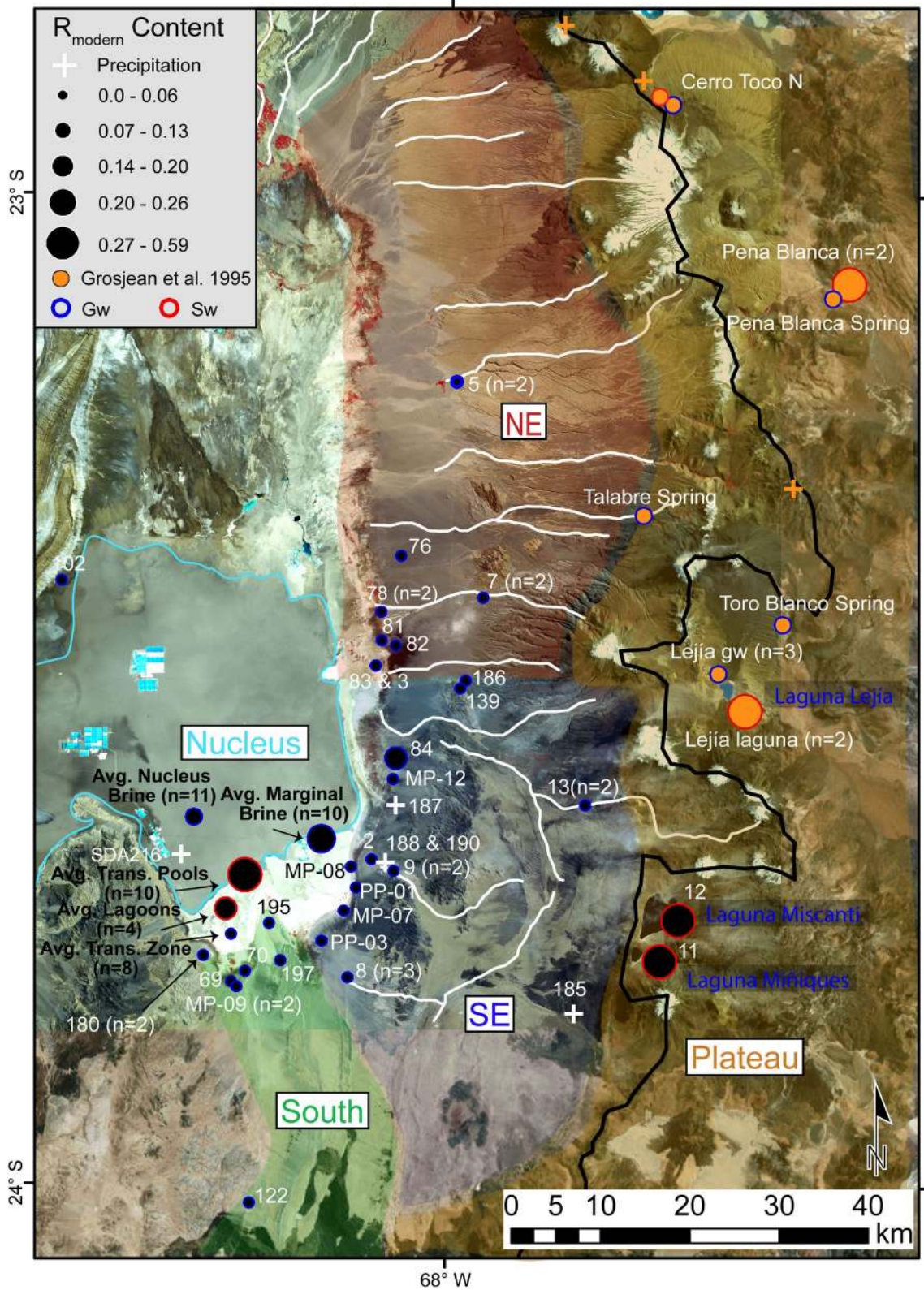


Figure 3. Modern water content in samples (n=87) proportional to circle size. Shaded areas are inflow water zones. Data from Grosjean et al. (1995) are orange. Circles in Nucleus and Transition Zone represent averages of water bodies. Surface waters (sw) are outlined in red, groundwaters (gw) in blue.

265 scale bias from ENSO conditions not the average (Houston, 2007). We assume this meteoric
 266 input value is representative of average precipitation from about 1990 to present because the
 267 bomb peak signature is no longer resolvable after that date in the southern hemisphere, and also
 268 representative of average precipitation before the mid-1950's since the bomb peak had not yet
 269 occurred (Houston, 2007; Jasechko, 2016). Water recharged in 1955 prior to the bomb peak with
 270 a ^3H content of 3.23 ± 0.6 TU would have between 0.08 and 0.11 TU in July 2018 (Stewart et al.,
 271 2017).

272 This pre and post-bomb *background* ^3H production temporally constrains the meteoric
 273 input value, but there is also a potential source of ^3H that is produced within the aquifer from ^6Li
 274 neutron flux. This potential *in-situ* production from water-rock interaction is generally assumed
 275 to be very small but given the Li-rich aquifer material in this region we consider it a potential
 276 factor in the maximum apparent *background* ^3H threshold (Boutt et al., 2016; Houston, 2007).
 277 By assessing the ^3H content of Salar de Atacama nucleus brine samples which have been
 278 determined to be $\gg 60$ years old through other methods, we can establish the cutoff for this *in*
 279 *situ* production to be approximately 0.15 TU (Boutt et al., 2016; Houston, 2007; Munk et al.,
 280 2018). Therefore, values less than 0.15 TU are essentially indistinguishable from 0.0 TU due to
 281 this potential *in situ* production in waters containing effectively zero water volume recharged
 282 post-1955; waters below this threshold are interpreted to be ^3H -dead. Nearly all waters sampled
 283 in this analysis contain values of ^3H near zero and therefore contain small fractions of modern
 284 water if any; because of this, our objective is not to directly estimate discrete MRT distributions
 285 or the “percent modern” component of these waters (Cartwright et al., 2017). Instead, we
 286 quantify the relative amount of modern water present to constrain connections to modern
 287 meteoric inputs among the surface and groundwater bodies and connections between these
 288 systems.

289 All ^3H samples are allocated to nine distinct water “bodies” representing the major water
 290 compartments in the basin. These groundwater and surface water bodies, corresponding closely
 291 to those discussed by Boutt et al. (2016) and Munk et al. (2018) are hydrogeologically distinct,
 292 formed and sustained by a unique set of hydrological processes. Waters are grouped into (Figure
 293 3): Nucleus Brines, a very dense brine (>200 mS/cm SC) within the core of the evaporite aquifer;
 294 Marginal Brines, a dense brine in the transition between the Nucleus Brines and fresher
 295 Transition Zone waters; the Transitional Pools, highly saline (>200 mS/cm SC) surface waters at
 296 the margin of the nucleus surficial halite deposit, in the southeast zone of the salar these waters
 297 occupy about 0.2 km² of surface area. Landward of these Transitional Pools are several large

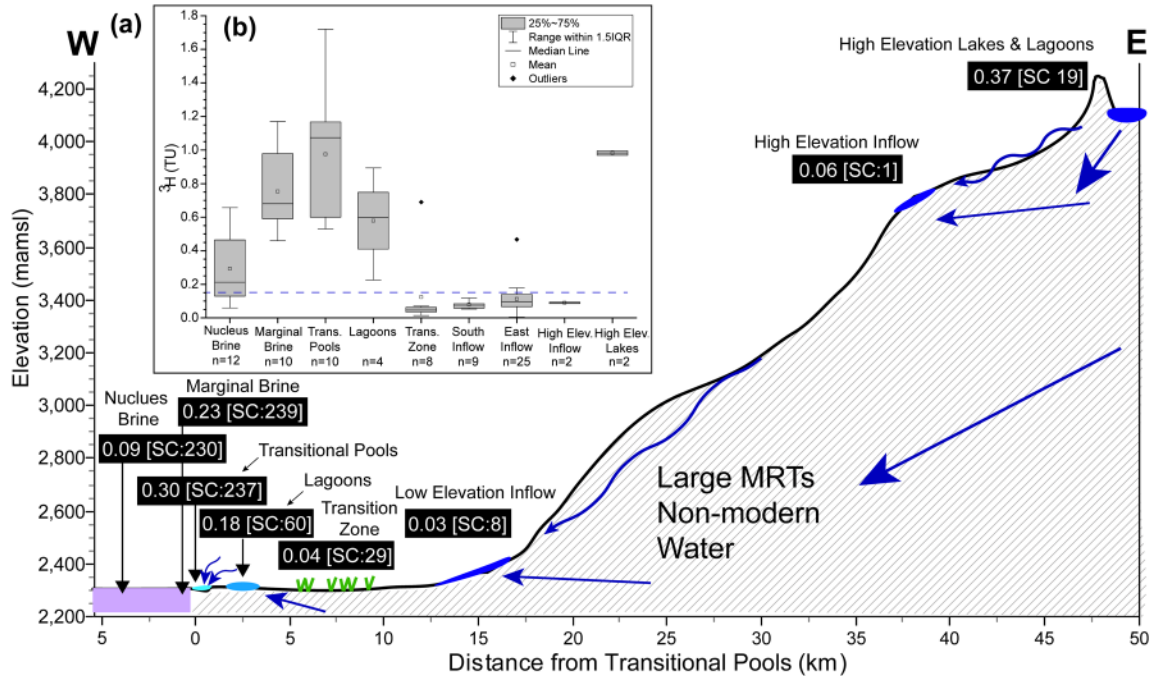


Figure 4. (a) Modern water proportion (R_{mod}) among groundwater and surface water bodies along a transect of the eastern Salar de Atacama margin. South Inflow and East Inflow waters are averaged as a single low elevation inflow water body. Mean R_{mod} value of each water grouping (in black rectangles) and mean Specific Conductivity (SC) in mS/cm. **(b)** Tukey box plot of 3H content (TU) in these water bodies. Blue dashed line is the theoretical maximum limit (0.15TU) of background 3H produced in-situ by water-rock interaction.

298 brackish Lagoons, shallow surface water bodies which occupy about 0.5 km² and host important
 299 wildlife such as flamingos and brine shrimp. Transition Zone waters are shallow brackish
 300 groundwaters within the surficial gypsum dominated zone between the nucleus and the edge of
 301 the basin floor; South Inflow and East Inflow are fresh groundwater discharge waters entering the
 302 basin below ~3000 mamsl; High Elevation Inflow waters are fresh groundwater discharge higher
 303 on the eastern slope of the basin; and the High Elevation Lakes are fresh-to-brackish lake waters
 304 just outside the watershed divide.

305 All 3H data for each of these water bodies are summarized in Tukey Box plots and plotted
 306 along a transect through the eastern basin margin (Figure 4). Results show that waters discharging
 307 along the margin have values indistinguishable from zero as nearly all fall fully below the
 308 background threshold described above. The only two samples (73 & 84) which have higher
 309 values and the few that are borderline above the background, in the Transition Zone and the East
 310 Inflow are in the proximity of preferential flow paths related to rapid infiltration of modern
 311 precipitation into permeable alluvial fans, a process indicated by Boutt et al. (2016). The data
 312 from high elevation lakes Miñiques and Miscanti (samples 11 & 12) as well as other surface
 313 waters at high elevation (Laguna Lejía & Pena Blanca) show much higher values, similar to the

Elevation of Lakes (mamsl):	4150	Hydraulic Conductivity [K]:				
		K= 15.5 m/d		K=5.0 m/d	K=1.0 m/d	K=0.01 m/d
Sample Site (name)	Elevation (mamsl)	Distance from Lakes (km)	v (m/d)	v (m/d)	v (m/d)	v (m/d)
13 (Socaire)	3606	12	5.0	1.6	0.32	0.0032
9 (Peine)	2450	29	6.5	2.1	0.42	0.0042
8 (Tilomonte)	2373	33	6.0	1.9	0.38	0.0038
84 (Truck)	2329	34	5.9	1.9	0.38	0.0038
Sample Site (name)	Hydraulic Gradient [dh/dl]		MRT (yrs)	MRT (yrs)	MRT (yrs)	MRT (yrs)
13 (Socaire)	0.045		7	20	101	10146
9 (Peine)	0.059		12	38	190	18962
8 (Tilomonte)	0.054		15	47	235	23490
84 (Truck)	0.054		16	49	243	24333
Sample Site (name)	Distance from Lakes (km)	³ H* (TU)	MRT w/Lake Water Input (yrs)	MRT w/Precipitation Input (yrs)	v (m/d)	
					Assuming ³ H- Calculated MRT (w/ lake water)	Assuming ³ H- Calculated MRT (w/ precip.)
Precipitation [N _o]	0	3.23	-	-	-	-
11 & 12 (Miñ./Mis.) [N _o]	0	0.67	-	-	-	-
13 (Socaire)	12	0.07	40	68	0.8	0.5
9 (Peine)	29	0.04	48	76	1.7	1.0
8 (Tilomonte)	33	0.08	37	65	2.5	1.4
84 (Truck)	34	0.32	13	41	7.2	2.3

Table 1. Calculations of transit time estimates assuming piston flow and a decay constant. The High elevation lake water ³H value and modern meteoric water are used as input ³H values. These input values were decayed and seepage velocities (v) estimated with aquifer properties (K & θ) from Houston (2007) and a plausible range of values. Velocities were calculated by piston flow transit times, then the MRT of waters were estimated under these conditions.

314 average of Transitional Pool waters. Nucleus Brine waters are predominantly composed of pre-
 315 modern groundwater with a small component of modern water in some samples, the Transition
 316 Zone waters are entirely pre-modern while the Lagoons have a large component of pre-modern
 317 water but some samples contain a substantial amount of modern water.

318 The spatial coverage and density of samples across the eastern margin, considering the
 319 focused nature of groundwater discharge in the basin gives confidence that shallow inflow to the
 320 salar is well-represented by this analysis and that nearly all of it is composed of pre-modern
 321 water. It is also apparent that surface waters (Lagunas Miñiques, Miscanti, Lejía, and the
 322 Transitional Pools) have an analogous signature of about 0.30-0.40 R_{mod}. This consistent
 323 signature highlights and defines the substantial contrast between the surface water system and
 324 groundwater system (surface water sample “Cerro Toco N” is the exception to this, likely
 325 primarily composed of water sourced from the “Cerro Toco N” groundwater just upgradient)
 326 (Figure 3). The interaction of these surface and groundwater systems serve to illuminate
 327 hydrological mechanisms governing the system as a whole and constrain the distribution of
 328 modern water within its sub-systems.

329 Since the groundwater can only be directly measured at discrete points and processes in
 330 the thick vadose zone are not easily constrained, simple analytical representations with a range of
 331 plausible hydrologic properties can facilitate interpretation of dominant processes controlling

332 flow paths, MRTs and sources of groundwater inflow. Along a cross-section from the
 333 Transitional Pools to the High Elevation Lakes (Figure 4) we estimate the MRT of sampled
 334 groundwater discharge assuming a shallow flow path (<100 m), piston flow and a plausible range
 335 of hydraulic properties (Table 1). The MRT estimates for each groundwater discharge site were
 336 calculated independently using the observed ³H values, a range of seepage velocities and
 337 measured hydraulic gradients (dh/dl) (Table 1).

338 If we first assume the ³H value of recharge water lies somewhere between modern
 339 precipitation and high elevation surface waters (as focused recharge from these waters bodies is
 340 thought to be important), it will decay according to this formula as it moves downgradient; where
 341 t = time, N = sample ³H value, N_o = initial ³H value and λ = the decay constant of ³H:

342
$$t = \frac{\text{Ln}(N/N_o)}{-\lambda}$$

343 We then estimate how long it would take for that water to decay enough to match the ³H value
 344 measured in groundwater discharging downgradient. This MRT is not intended to physically
 345 replicate the complexity of groundwater transport but paired with a range of seepage velocities,
 346 this places critical constraints on plausible MRTs. Using estimated effective porosity (θ) and a
 347 range of hydraulic conductivities (K) including values previously determined by Houston (2007)
 348 in a basin just north of Salar de Atacama, we calculated a seepage velocity for each sample site:

349
$$v = (K/\theta) \times (dh/dl)$$

350 We then determined the seepage velocity required for each flow path to reflect the MRT at each
 351 site estimated by simple ³H decay. Lastly, we calculated the MRT for each sample using these
 352 estimated seepage velocities.

353 These results indicate that simple piston flow and ³H decay predict a sizeable portion of
 354 young water not observed at these sites and would require seepage velocities much greater than
 355 would be reasonable in this environment. Two factors would suggest that actual MRTs of these
 356 waters resemble something closer to those predicted with the lowest velocities in Table 1. ³H
 357 values in inflow waters are well below the background production envelope but are rarely zero,
 358 therefore the value used for those sites may be artificially high as some or all of the ³H in these
 359 waters is potentially derived from *in situ* production or analytical uncertainty while its modern
 360 water content may, in fact, be approaching zero. The thick vadose zones in this environment may
 361 require hundreds of years or more for water to infiltrate (Herrera et al., 2016; Walvoord et al.,
 362 2002) leading to effective seepage velocities much smaller than reasonable hydraulic conductivity

363 values in Table 1 would predict. Together this suggests that the low ^3H activities at these
 364 groundwater discharge sites cannot be explained by modern high elevation recharge flowing
 365 downgradient and becoming low elevation discharge within modern time frames; under the most
 366 plausible hydrogeologic conditions, it likely requires hundreds to thousands of years for high
 367 elevation recharge to reemerge as springs and diffuse groundwater discharge in the basin.

368 4.2 Oxygen ($^{18}\text{O}/^{16}\text{O}$) and Hydrogen ($^2\text{H}/^1\text{H}$) Ratios in Water

369 In this groundwater-dominated system, isotopic signatures of individual samples are
 370 primarily a reflection of its source water mixture and flow path characteristics. Comparing
 371 signatures in each discharge zone (N, NE, SE, and S) and recharge zone (North Divide, NE
 372 Divide, SE Divide, North Plateau, South Plateau-N and South Plateau-S) we can address
 373 important questions regarding dominant hydrological mechanisms governing the larger orogenic-
 374 scale groundwater system. It is important to note that the western half of the basin is not included
 375 in our analysis of the Salar de Atacama system because actual inflow from that region is
 376 negligible when compared to the other zones, accounting for less than 1% of the total (Munk et
 377 al., 2018) (Figure 2).

378 $\delta^2\text{H}$ data from the major groundwater discharge sites (springs) in the NE and SE zones
 379 measured seasonally over a nearly 7-year period and more sporadically back to 1969 show

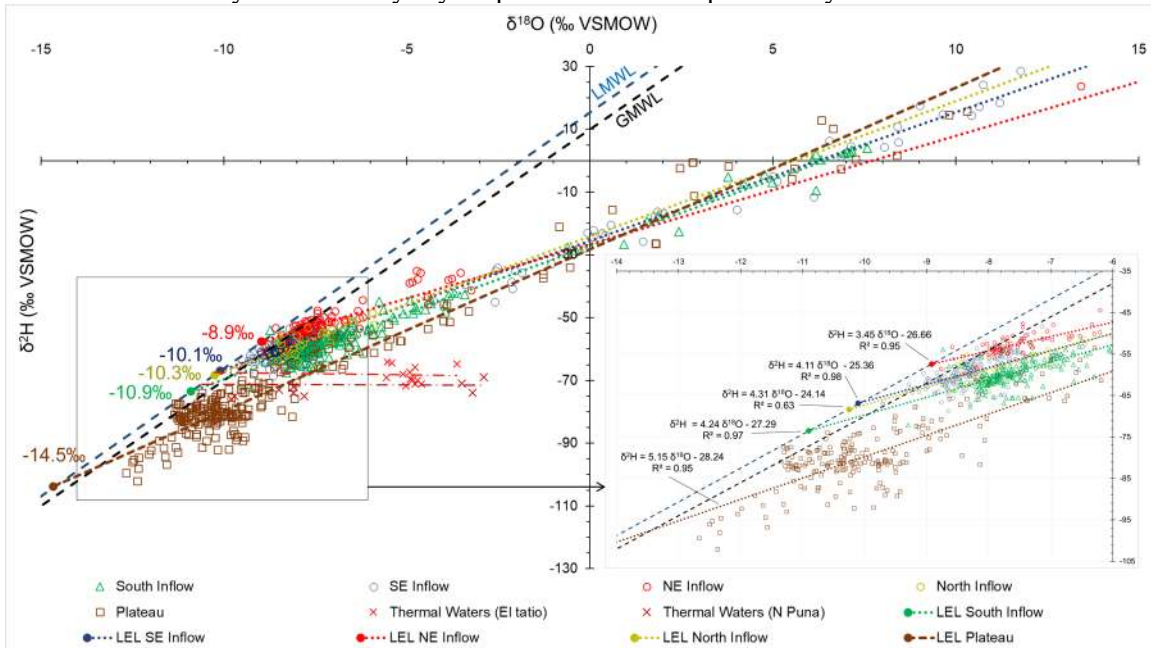


Figure 5. $\delta^{18}\text{O}$ and $\delta^2\text{H}$ of water from the Salar de Atacama regional watershed ($n=889$). Colors correspond to the three inflow zones labeled in Figure 2, brown points are all plateau waters. The meteoric source water isotopic signature is estimated for each zone where the LEL intersects the Local Meteoric Water line (LMWL) from Chaffaut et al. (1998). High-temperature waters from the El Tatio thermal field and northern Puna region indicated by red Xs.

380 consistent values with some correlation to large local precipitation events but the responses are
381 short-term (Figure S2). The documented major precipitation events in March 2012 and March
382 2015 appear to show negative deviations of 3-5‰ in $\delta^2\text{H}$, after which data revert to the long-term
383 trend in a few months. This suggests a signature of local meteoric infiltration is observed at these
384 sites below 3000 mamsl but is largely restricted to short time-scales, longer flow path waters are
385 the principal control on isotopic values of inflow water. Data from the sample sites within the NE
386 and SE zones have a mean standard deviation of 2.2‰ and 2.8‰ in $\delta^2\text{H}$ respectively, reflecting
387 variability between sites and the short-term influence of local recharge pulses. Stream gauge data
388 at the Spring-fed streams also show influence from local recharge events but revert to a consistent
389 long-term average value within a month or two (DGA, 2013). Since this analysis utilizes a large
390 dataset collected over more than 20 years, we are confident that our analysis of environmental
391 tracers reflects the long-term average discharge signal of the groundwater system.

392 All $\delta^2\text{H}$ and $\delta^{18}\text{O}$ data analyzed in this work are presented in Table S3, and are plotted in
393 $\delta^2\text{H} - \delta^{18}\text{O}$ space along the GMWL and the modern Local Meteoric Water Line (LMWL) in
394 Figure 5 (Chaffaut et al., 1998). To a first order it is apparent that a linear fit of all these data
395 forms a line which is offset below but parallel to the LMWL; this phenomenon has been observed
396 by several other workers in this basin and in other arid basins in the central Andes and worldwide
397 (Aravena, 1995, 1999; Boschetti et al., 2007; Fritz et al., 1981; Koeniger et al., 2016; Margaritz et
398 al., 1989). Also evident in these data is a bimodal distribution; one cluster has relatively depleted
399 $\delta^2\text{H}$, centered around -80‰ and the other around -60‰. Distinctions can also be identified
400 between zones of inflow which indicate important spatial differences in discharge within the
401 Salar de Atacama watershed.

402 The strong influence of kinetic fractionation due to evaporation in this region allows for
403 back-calculation of the expected meteoric source waters for each of these zones (Text S4). By
404 defining linear regressions of water data in each zone (Local Evaporation Lines (LEL)) we can
405 predict the meteoric source $\delta^{18}\text{O}$ and $\delta^2\text{H}$ signature while also determining the slope characteristic
406 of evaporative fractionation in each. Coefficients of determination (R^2) show these LEL describe
407 the data well (0.95-0.98), except in the North zone (0.63) for which there is less confidence due to
408 a relative lack of data ($n=24$). The four inflow water zones are defined by slopes of 3.5 (NE), 4.1
409 (SE), 4.2 (S) and 4.3 (N) while plateau waters show a steeper slope of 5.2 (Figure 5). These
410 values are consistent with empirically derived LEL from this region and similar environments
411 (Aravena, 1995, 1999; Boschetti et al., 2007, 2019; Ortiz et al., 2014; Scheihing et al., 2018).
412 Shallower slopes reflect the higher average annual temperatures and lower relative humidity of

413 the lower elevations, the steeper slope of high-altitude plateau waters reflects the higher average
 414 relative humidity and lower temperatures there and associated smaller kinetic effects. Predicted
 415 source waters derived by projecting these regressions to their intercepts with the LMWL show
 416 that the meteoric source of the plateau water is substantially more depleted in $\delta^{18}\text{O}$ and $\delta^2\text{H}$ than
 417 those of discharge waters within the basin. Inflow $\delta^{18}\text{O}$ signatures are higher by about 5.6‰
 418 (NE), 4.4‰ (SE), 4.2‰ (N) and 3.6‰ (S) than average plateau waters. We can, therefore, deduce
 419 that substantial hydrogeological distinctions exist between these two systems.

420 To refine the distinctions among recharge waters and to relate these characteristics
 421 spatially we compare isotopic signatures of the three recharge zones on the plateau and the three
 422 recharge zones in the region straddling the divide. Again, plotted in $\delta^2\text{H} - \delta^{18}\text{O}$ space we compute
 423 the predicted meteoric source of each recharge zone (Figure 6). These results show that waters of
 424 the divide predict source waters comparable to those discharging directly downgradient in the
 425 basin, implying that the predominant source signature of these waters is largely analogous. In
 426 comparison, the three zones on the plateau show substantially lower $\delta^{18}\text{O}$ and $\delta^2\text{H}$ signatures
 427 suggesting these waters have a different meteoric source from both the inflow waters and the
 428 divide waters. The zone covering the largest area of any (North Plateau) appears to be the most
 429 distinct from the Salar de Atacama watershed inflow with $\delta^{18}\text{O}$ values between 5.2‰ and 7.2‰
 430 lower. Further statistical scrutiny of these data provides a better definition of these distinctions.

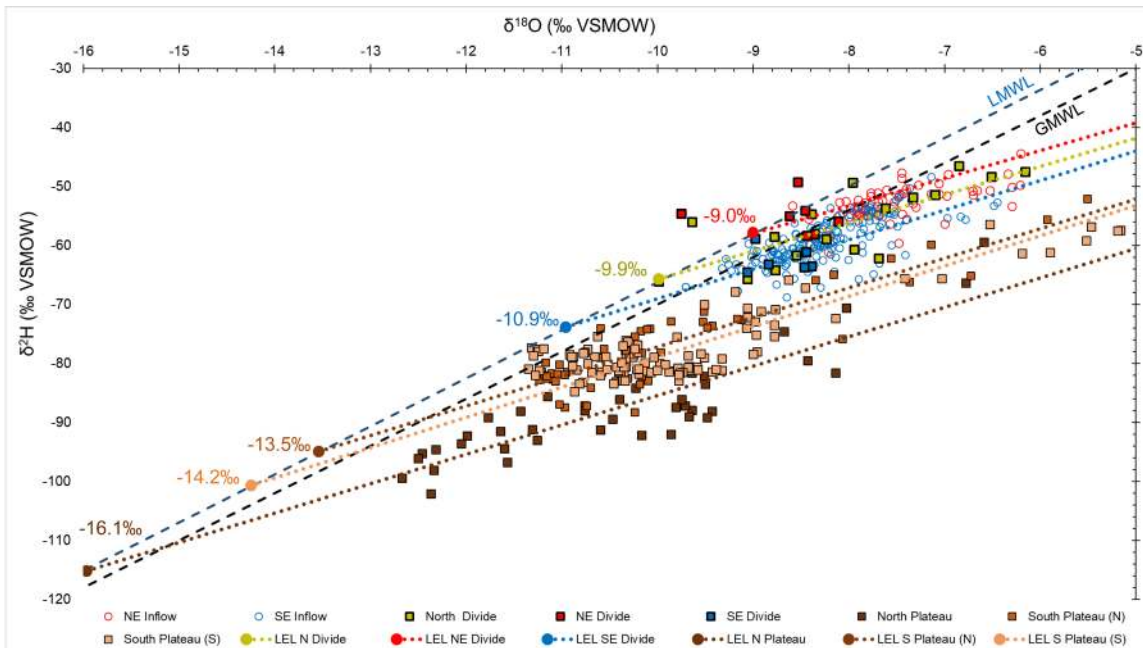


Figure 6. $\delta^{18}\text{O}$ and $\delta^2\text{H}$ of water from the plateau and divide recharge zones. Inflow waters (NE and SE zones) are red and blue points displayed for context. Predicted meteoric source waters from LEL intercept with LMWL are colored numbers.

431 $\delta^{18}\text{O}$ data from all zones were filtered with the deuterium-excess (d-excess) parameter
 432 and summarized statistically (Figure S3). Separating samples with a d-excess less than zero is
 433 considered the optimal point for removing most kinetic influences while maintaining the
 434 maximum number of samples uninfluenced by evaporative effects (Jasechko et al., 2014).
 435 Removing the kinetic evaporative influence from our dataset allows for direct comparison
 436 between inflow waters by including only those most representative of their original meteoric
 437 source. This analysis provides further evidence of the large statistical distinctions between all
 438 Salar de Atacama inflow water and waters on the plateau, also that there is less apparent
 439 distinction between the inflow and the divide waters. We find the mean $\delta^{18}\text{O}$ value of NE inflow
 440 zone water is about 1.3‰ higher than the divide waters upgradient, the SE inflow water values
 441 are about 0.4‰ higher than its corresponding divide waters and the N zone waters appear
 442 analogous to its corresponding divide waters. There is also a clear statistical distinction between
 443 the NE and SE inflow waters, one which is exhibited by the calculated meteoric source showing
 444 the mean $\delta^{18}\text{O}$ value of NE waters is about 1‰ higher than the mean SE waters. This suggests
 445 meaningful differences between sources and/or groundwater mechanisms governing the NE and
 446 SE inflow.

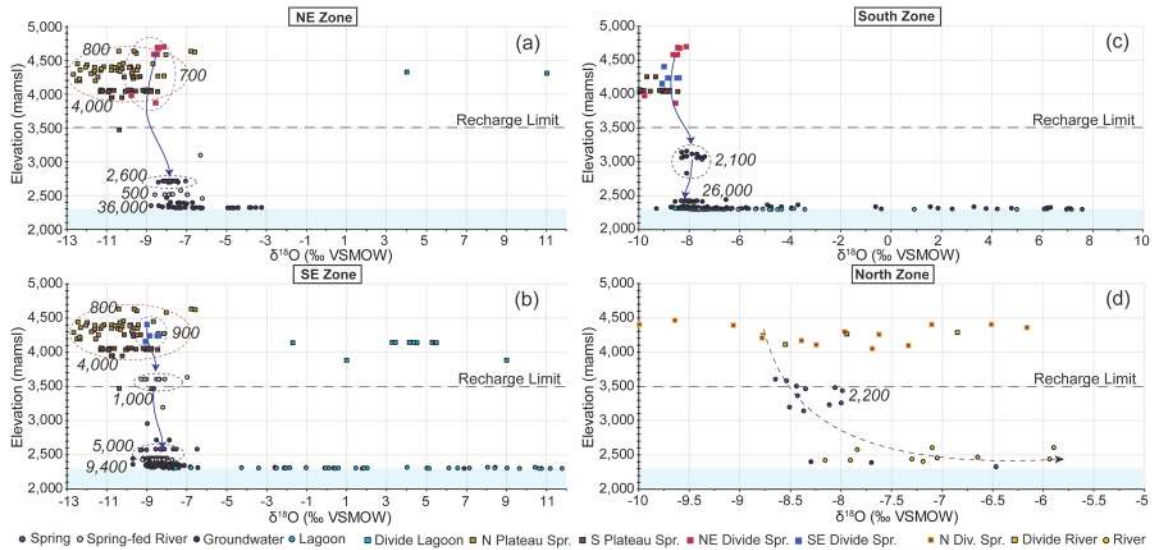


Figure 7. $\delta^{18}\text{O}$ in waters from each zone plotted against sample elevation. Recharge limit line denotes elevation below which no significant recharge occurs; Houston (2009), Scheihing et al. (2018) and others have shown for this region the limit lies at $\sim 120\text{mm}$ of precipitation per year (Figure 1). Blue shaded envelope represents the salar evaporite aquifer below the basin floor. Specific Conductivity ($\mu\text{S}/\text{cm}$) of sample groupings in italics. Ellipses in (a), (b) and (c) indicate descriptive groupings discussed in text and blue arrows indicate general hydrochemical evolutionary pathways. Dashed arc in (d) indicates the predicted trend of isotopic evolution in a river system. Water types and locations are labeled in legend (Spr.=Spring water).

447 These same d-excess filtered data from each compartment were compared using an
 448 unequal variances t-test (Welch’s test) to assess the null hypothesis that samples within each zone
 449 represent waters from the same population. $\delta^2\text{H}$ and $\delta^{18}\text{O}$ values of these water groupings were
 450 compared: All Divide - All inflow (N, NE, SE, S); All Plateau – All Inflow; All Divide – All
 451 Plateau; NE – SE and SE – S. Results show strong statistical difference ($P < 0.0001$) between all
 452 these zones except for All Divide – All inflow ($P=0.035$) for both $\delta^2\text{H}$ and $\delta^{18}\text{O}$ and SE – S
 453 ($P=0.164$) for $\delta^2\text{H}$ values only. Divide waters and inflow waters are not statistically distinct in
 454 terms of $\delta^2\text{H}$ or $\delta^{18}\text{O}$, S and SE waters are distinct with respect to $\delta^{18}\text{O}$ but not distinct with
 455 respect to $\delta^2\text{H}$, which indicates another hydrological process may be influencing waters in the
 456 South zone.

457 To compare groundwater flow paths into the basin, we trace the isotopic evolution of
 458 waters moving through each inflow zone. Figure 7 shows $\delta^{18}\text{O}$ by sample elevation for each
 459 inflow zone and the recharge waters upgradient of them. Waters in each zone show a general
 460 trend of increasing salinity with decreasing elevation toward the Salar de Atacama basin aquifer.
 461 This trend is expected as more dissolved solids can be accumulated in groundwater from rock
 462 weathering and re-mobilization of residual salts present in the aquifer material. While a
 463 substantial increase in salinity downgradient indicates waters are evolving geochemically, $\delta^{18}\text{O}$
 464 values only increase by about 0‰-2‰ between divide recharge and discharge waters. This has
 465 been observed in previous work in this region showing increasing salinity with no isotopic
 466 evolution reflects “salinization” of fresh groundwater inflows, not evaporative enrichment (Fritz
 467 et al., 1978; Risacher et al., 2003). The evolution observed in the NE, SE and S waters show that
 468 groundwaters discharging near the salar margin have a direct relationship to that of groundwaters
 469 in the divide recharge area upgradient but not the majority of the plateau waters. The overlap that
 470 occurs between some plateau waters and divide waters, especially in the SE suggests there is at
 471 least some connection between portions of the plateau and Salar de Atacama inflow. The south
 472 zone displays similar characteristics to the NE and SE but also a slight decrease in $\delta^{18}\text{O}$ values
 473 from the groundwater in the central MNT aquifer to discharge near the Tilopozo wetland. In the
 474 N zone where two large perennial rivers flow to the basin floor, waters follow a trend more
 475 typical of a surface watershed where the lower reaches are steadily isotopically evolved due to
 476 strong evaporative fractionation. $^{87}\text{Sr}/^{86}\text{Sr}$ data presented by Munk et al. (2018) indicate that
 477 some of the sub-basins (e.g. Miscanti) on the divide and plateau have direct geochemical
 478 connections to downgradient inflow areas, while others appear quite disconnected. Since actual
 479 recharge is insignificant where annual precipitation is less than 120 mm/year (equating to an

480 elevation of ~3500 mamsl), these results suggest the predominant source of inflow is upgradient
481 groundwaters, not local inputs (Houston, 2009; Houston, 2007; Houston & Hart 2004).

482 4.3 Constraining Modern Meteoric Inputs

483 Air mass tracking of major precipitation events reveal macro-scale features of the modern
484 climate regime and allow for comparison between meteoric recharge inputs to the plateau and
485 ultimately the inflow zones (Figure S4). Our results indicate that nearly all precipitation is
486 derived from either the northeast or east and any distinctions in meteoric input signatures to this
487 system are more a consequence of localized convective and orographic effects than distinctions
488 between initial moisture source. Prominent orographic barriers exist along the length of the
489 watershed divide and along an NW to SE trending chain of volcanoes to the east of Laguna
490 Miñiques which may develop distinctive average meteoric input signatures among recharge zones
491 and inflow waters to the Salar de Atacama basin.

492 5. Discussion

493 Our integrated analysis of isotope systematics in the waters of Salar de Atacama regional
494 watershed defines the spatiotemporal dimensions of dominant sources and flow paths, the
495 distribution and degree of connection among water bodies, sub-catchments and perched basins on
496 the Altiplano-Puna plateau, and distinctions between the modern and paleo-hydrological systems.
497 We show that inflow to the basin is not predominantly composed of recharge on the plateau,
498 modern recharge (<60 years old) on the high elevation watershed divide or local, modern inputs
499 within the watershed. We conclude this based on the following lines of evidence: (i) there are
500 substantial distinctions between the $\delta^{18}\text{O}$ and $\delta^2\text{H}$ signatures of Salar de Atacama inflow water
501 versus waters on the plateau; (ii) nearly all waters discharging in the basin are composed of pre-
502 modern water, and modern water that exists is limited and focused in nature, and (iii) based on
503 the physical properties of this system, modern groundwater recharge within the watershed and on
504 the divide would likely take hundreds of years or more to become groundwater discharge in the
505 basin. Therefore, the draining of transient storage in the groundwater system over large time
506 scales must be a critical component of the present water budget. We also propose that the influx
507 of solute-rich underflow from high elevation basins over long time-scales, predominantly in the
508 southern and eastern regions is an important mechanism to account for the large solute (Na and
509 Cl) imbalances in hydrological budgets (Munk et al., 2018). These governing mechanisms are
510 defined in a fully integrated conceptual model of this system as it currently exists, placing critical
511 constraints on fundamental hydrological processes controlling orogenic-scale groundwater

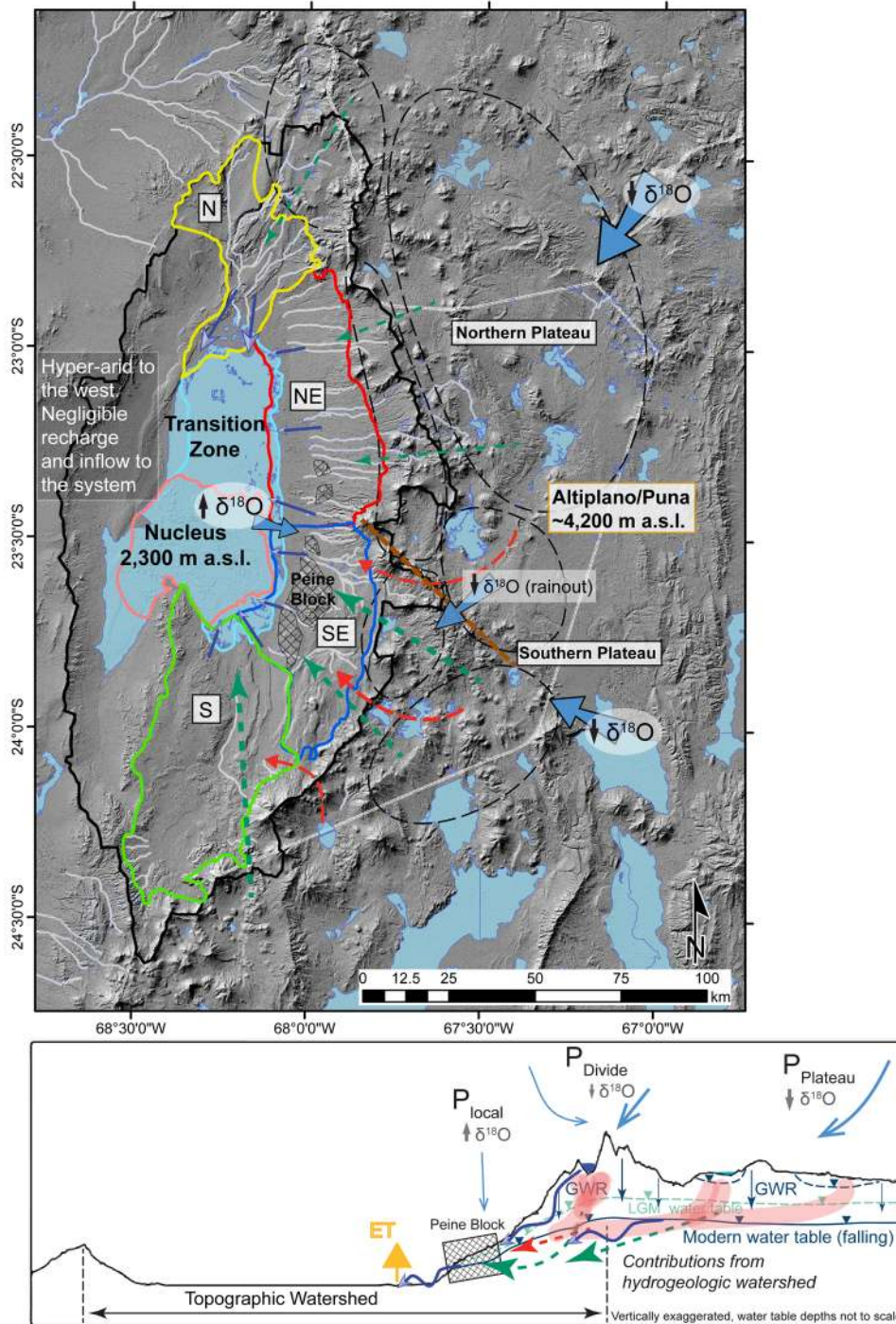


Figure 8. Conceptual model of the Salar de Atacama regional groundwater system, major mechanisms governing the contemporary hydrologic system and their relative influence (adapted from Corenthal et al. 2016). In plan view (a), solid light blue arrows represent the distribution of modern meteoric inputs and their signatures, the brown dashed line denotes a major orographic barrier to precipitation east of Miñiques and Miscanti lakes. Solid blue arrows represent inflows of modern recharge, green dashed arrows are major inputs of paleo-groundwater, red dashed arrows show hypothesized influx of solute-rich fluid. (b) Cross-sectional view of the SE zone shows the distribution and relative importance of these hydrological mechanisms. Blue lines are estimated position of the modern water table, green is the LGM water table and the corresponding flow paths of modern and fossil groundwater, red is solute-rich influx.

513 systems (Figure 8). Our results reveal novel insights about these large-scale systems and
514 provide a framework within which to address important unresolved questions in these basins
515 worldwide.

516 Analysis of ^3H , the long-term stability of isotopic signatures in groundwater discharge
517 and insignificant direct recharge occurring at low elevations indicate that inflows from the
518 southern and eastern margins of Salar de Atacama are principally composed of pre-modern
519 recharge. These inflow waters which represent a large portion of total water flux (~65%) and
520 solute flux into the basin are, principally, expressions of a regional hydrologic system decoupled
521 from modern inputs (Munk et al., 2018). Surface waters bodies at high and low elevations
522 (Laguna Miñiques, Miscanti, Lejía, and the Transitional Pools) have a consistent signature of
523 about 30% modern, reflecting a dynamic equilibrium between ^3H -rich modern recharge, ^3H -dead
524 groundwater inflows, and discharge fluxes. This consistent signature among these waters which
525 have direct connections to modern meteoric inputs highlights a clear contrast between surface
526 water systems and the groundwater system. The prevalence of pre-modern water observed in
527 inflow to the basin, the timing of past pluvial periods (>1000 yrs.), thick vadose zones (up to
528 1000 m or more) and the large scales over which these flow paths must develop reveal a
529 groundwater system which operates over time scales of 100-10000 years or longer. Taken
530 together, these results indicate that the Salar de Atacama hydrologic system is fundamentally
531 groundwater controlled and strongly compartmentalized by source and flow path over small
532 spatial and vertical distances.

533 Large infrequent precipitation events observed and described by Boutt et al. (2016) and
534 others which do infiltrate and move along preferential flow paths near the margin of the evaporite
535 deposit are governed by the presence of alluvial fans with high infiltration capacities and by sharp
536 saltwater-freshwater interfaces created by the dense brine of the evaporite aquifer. These
537 interfaces which exist near the surface in the transition zone are remarkably stationary and restrict
538 infiltration of fresher water, creating pathways of preferential flow on the margins of the salar
539 (McKnight, 2019). This modern meteoric water is directly reflected in the elevated ^3H values
540 observed in the Transitional Pools near the margin of the salar nucleus, in some areas of the
541 lagoons and in isolated shallow groundwater in some alluvial fans. The lagoons respond to this
542 focused infiltration and flow by occasionally flooding during extreme precipitation events near
543 the basin floor but largely return to their original shape and volume within months. This is
544 supported by the findings of Boutt et al. (2016) showing responses in the shallow brine aquifers
545 to large precipitation events on the salar are muted and short-lived and that the groundwater-

546 dominated lagoons show little permanent response to these events. Lagoon water ^3H
547 compositions show they are predominantly composed of pre-modern groundwater inflow and that
548 floodwater likely exists as a lens above the much denser lagoon water, focused and channelized
549 by the low permeability gypsum covering much of the transition zone. The few Transitional Pool
550 waters which were sampled just below the salar surface south of the open pools also contain
551 substantial amounts of this modern water as well as the lagoon sample “La. Brava B”, taken from
552 a shallow arm of the lagoon in the path of one of these focused flow paths. The waters along the
553 transition zone-nucleus margin are controlled by exchanges between these modern meteoric water
554 lenses and pre-modern groundwater inflow from below. The ^3H content of lagoon waters and
555 waters in the transition zone subsurface likely reflect the mixing of small volumes of this modern
556 water with much larger volumes of pre-modern inflow. Though the specific dynamics of these
557 lenses and their interaction with groundwater requires further inquiry, there is ample evidence
558 that modern water effectively bypasses the lagoons themselves in these lenses and migrates
559 toward the Transitional Pools where it dissolves and infiltrates through the porous halite units at
560 the nucleus margin.

561 Recent research of global climate change indicates that in this region of the Andes and
562 Preandean depression an increase in overall moisture and also large precipitation events is
563 predicted due to a southward shift in the South American Monsoon (Jordan et al., 2019;
564 Langenbrunner et al., 2019; Pascale et al., 2019). The substantial increase in extreme precipitation
565 events observed since 2012, with one 4-day event in February 2019 recording ~100mm of rain on
566 the salar surface which normally receives only 15 mm/year (personal communication with
567 Albemarle corp., July 2019) may, in fact, be a direct result of these large-scale climate changes
568 and are likely to continue. The recent observations of persistent surface water expansion in the
569 transition zone of Salar de Atacama (particularly the Transitional Pools) may also be a result of
570 these decadal-scale changes in meteoric inputs, not a direct result of extractions from the brine
571 aquifer or long-term changes associated with fluctuations in paleo-groundwater inflow.

572 Region-wide analysis of stable O and H isotope systematics reveal that each water inflow
573 zone is defined by a distinct combination of sources and flow paths relating directly to their
574 geology, meteoric inputs and connections to high elevation sub-basins beyond the watershed
575 divide. Our analysis shows important variations in spatiotemporal connectivity between these
576 high elevation zones and inflow to the basin which illustrates a heterogeneous and
577 compartmentalized regional flow regime. The results of HYSPLIT back trajectories and our
578 understanding of the modern climate regime show that differences in atmospheric source to

579 recharge and discharge zones are not significant and cannot explain the substantial differences in
580 isotopic signature we observe between inflow and recharge. Ultimately, meteoric water in the
581 system is derived almost entirely from the Amazon and Chaco basins to the east, as this moisture
582 traverses the Andean plateau it undergoes substantial rainout and recycling fractionation. The
583 average isotopic signature of meteoric waters in each zone and their associated groundwaters
584 reflect the orientation of their respective recharge areas in relation to the dominant moisture
585 sources and the topographic barriers they interact with. Specifically, the 1-1.2‰ higher $\delta^{18}\text{O}$
586 values observed in waters discharging from the NE zone relative to the SE zone is due to the lack
587 of rainout fractionation in precipitation reaching its major recharge areas and the fact that the NE
588 Divide zone is ~250m lower in average elevation than the SE Divide. With estimated $\delta^{18}\text{O}$ lapse
589 rates between -0.9‰ and -1.7‰ per km of elevation (Rohrman et al., 2014), the difference in
590 recharge elevation could account for only about 0.2-0.4‰ of this difference. The prominent
591 topographic barrier that exists to the east of the Miñiques and Miscanti lakes (controlled by the
592 COT fault system) may lead to consistent further isotopic depletion of precipitation in the SE
593 zone contributing areas (Pingel et al., 2019) (Figure 8). This is also reflected in the nearly 2.0‰
594 higher $\delta^{18}\text{O}$ values observed in the NE Divide waters relative to SE Divide waters.

595 The influence of snowmelt on groundwater recharge has been discussed as an important
596 control on the isotopic signature of groundwater in this region (Herrera et al., 2016). We argue
597 that since there are no permanent or deep seasonal snowfields in the entire region, snowfall is
598 distributed quite uniformly across the high altitudes and likely 20-30% of the snow is sublimated
599 before infiltrating, the signal of this snowmelt would not lead to systematic differences between
600 recharge zones or inflow zones not already discussed herein (Beria et al., 2018; Stigter et al.,
601 2018; Vuille & Ammann, 1997). In addition, the dominant moisture source and general climate
602 regime is not believed to have changed substantially through multiple pluvial periods during and
603 since the last glacial maximum (LGM), it was simply more amplified (Godfrey et al., 2003). This
604 suggests that the background precipitation isotopic signatures in each of these zones due to
605 orographic effects and moisture source likely has not varied substantially through multiple pluvial
606 periods. However, it would be expected that the isotopic signature of this pluvial recharge would
607 have a distinct signature which can be identified.

608 Oxygen and hydrogen isotope ratios in water data presented here consistently align
609 parallel to but below the LMWL and GMWL in $\delta^{18}\text{O}$ - $\delta^2\text{H}$ space, indicating another important and
610 consistent distinction between modern meteoric water and groundwater. A similar signal has
611 been identified in the Central Andes and in other arid regions for which two explanations have

612 been proposed: the continued evaporation of water during infiltration through the unsaturated
 613 zone (Barnes & Walker, 1989; Fontes & Molinari, 1975; Zimmerman et al., 1967) and a direct
 614 signature of pluvial groundwater recharge (Fritz et al., 1981; Magaritz et al., 1989; Meijer &
 615 Kwicklis, 2000). Laboratory and field measurements of diffuse recharge in arid environments
 616 estimate that d-excess excursions in groundwater recharge can range between 0‰ to as much as -
 617 10‰ relative to the initial meteoric water (Barnes & Allison, 1988; DePaolo et al., 2004). In this
 618 region it is likely that the actual influence of this process is less than the maximum due to the fact
 619 that much of the recharge occurring here is focused (i.e. through fractures and at permeability
 620 contrasts) not diffuse, is heavily biased to larger precipitation events and occurs at the highest
 621 elevations where there are steeper LEL slopes than in most arid environments. Recharge waters
 622 from wetter periods in the past would fall along a different GMWL than the modern due to
 623 differences in composition of the global ocean and the substantially higher relative humidity in
 624 this region would shift the LMWL (Meijer & Kwicklis, 2000). This paleo-meteoric water line
 625 during the most recent pluvial periods, for instance, is predicted to have a y-intercept of between
 626 0 and 5, resulting in a d-excess excursion from the modern LMWL of between -10‰ and -15‰
 627 (Clark & Fritz, 1997; Fritz et al. 1981). The observed excursion (lc-excess) in the SE and NE
 628 zone groundwaters and spring waters show an average of -10‰, the South zone -19‰ and high
 629 elevation waters -16‰ (Landwehr & Coplen, 2006). While both of these processes likely have
 630 some influence on these observed isotopic shifts, the magnitude of the shift we document
 631 suggests that only a portion of this signal can be accounted for with vadose zone fractionation.
 632 We argue that this signature has a fingerprint of pluvial period groundwater recharge now
 633 draining from storage. A similar signature has been identified in groundwater isotope data in arid
 634 regions worldwide where large water and solute imbalances have also been observed, this may
 635 indicate the relative influence of draining paleo-recharge and help explain these imbalances.

636 $\delta^{18}\text{O}$ and $\delta^2\text{H}$ data from the South zone and the plateau zones appear to be skewed further
 637 off the LMWL (illustrated by their large lc-excess) giving these waters an apparent LEL slope
 638 shallower than would be expected (Figure 5). Additional fractionation caused by isotopic
 639 exchange from interactions between silica-rich rock and high-temperature fluids has been
 640 documented in this and other regions with high tectonic activity, tending to evolve waters along a
 641 nearly horizontal slope in $\delta^2\text{H} - \delta^{18}\text{O}$ space (Cortecci et al., 2005; Rissmann et al., 2015).
 642 Thermal waters from two sites in the El Tatio geothermal field, northern Chile (Cortecci et al.,
 643 2005) and Jujuy Province on the northern Puna plateau of Argentina (Peralta Arnold et al., 2016)
 644 provide approximate end-members with which to identify this influence (Figure 5). This shift
 645 superimposed on the data is apparent in the plateau and South zone waters by the considerable

646 skew off the LMWL towards this geothermal end-member. This process may help explain some
647 of the apparent isotopic distinctions seen in the South zone waters with respect to the other inflow
648 zones. Waters discharging in the South may, in fact, be more similar to the SE waters in source
649 but are further fractionated as they flow towards the basin by remnant heat from the Socoma
650 volcano, as indicted by Rissmann et al. (2015).

651 This work describes a large-scale integrated groundwater system where water is
652 transported over long time-scales and across a vast regional catchment, therefore it is also likely
653 that groundwater discharging to the Salar de Atacama basin is connected to some degree with the
654 many internally drained sub-basins at high elevation (Figure 8). This solute-rich interbasin flow
655 has been suggested by Grosjean et al. (1995), Munk et al. (2018) and Rissmann et al. (2015)
656 among others as an important source of solutes to the Salar and explains in large part, the excess
657 mass accumulated in the evaporite deposit. Three pieces of evidence in our results support this
658 interpretation: (i) the regions we call the Divide zones, straddling the Salar de Atacama watershed
659 divide have water isotope signatures that are consistent with groundwater discharge in the basin
660 and therefore also consistent with infiltration occurring within these perched watersheds; (ii) the
661 density of active salars and salt lakes close to the watershed divide, bounded to the north by the
662 COT fault system is much higher than in the northern half of the basin; and (iii) the waters in the
663 South and SE zone have much higher concentrations of conservative solutes than other parts of
664 the basin as discussed by Munk et al. (2018).

665 **6. Conclusions**

666 Our exhaustive examination of isotopic systematics in this orogenic-scale groundwater
667 system defines a regionally integrated system in which transient draining of groundwater from
668 storage over long time scales is a fundamental control. This fossil water still moving through the
669 system reflects catchment-wide dynamic responses to multiple large-amplitude climatic
670 fluctuations over 10^2 - 10^4 year time scales and represents a critical portion of the present water
671 budget of the Salar de Atacama basin. We show that modern water in the system is limited,
672 predominantly confined to shallow preferential flow paths near the margin of the salt flat and in
673 alluvial fans. The movement of modern water and fossil water in the system is highly
674 compartmentalized over small spatial and vertical distances. In addition, we show that
675 groundwater recharge on much of the Altiplano-Puna plateau (>100 km from the salar) is
676 decoupled from groundwater currently entering the basin but that the high elevation area
677 straddling the watershed divide and the sub-basins just beyond constitute the primary recharge
678 area to the basin. This work offers compelling evidence that evaluations of water use and

679 sustainability in this region must integrate modern observations with an understanding of
680 processes operating across large spatial and temporal scales. As an archetype of arid continental
681 basins worldwide, these mechanisms, to varying degrees are critical for reconciling observed
682 imbalances and must be spatiotemporally constrained in any model representing these systems.
683 This work provides a framework within which to identify these mechanisms and connections at
684 the catchment scale thereby allowing water resources to be more responsibly developed
685 worldwide.

686 While this work significantly advances our understanding of the spatiotemporal dynamics
687 controlling these large groundwater systems, outstanding questions relating to catchment-wide
688 response times to changes in recharge and water tables remain. Specifically, how connected are
689 high elevation recharge areas and sub-basins near the divide to groundwater discharge in the Salar
690 de Atacama basin, what are the response times to these changes and how do they vary across the
691 system. To address these questions, we propose a few main lines of further inquiry: i) filling in
692 gaps in the transit time distribution of groundwaters throughout the system to further discretize
693 fossil waters >1000 years old; ii) detailed hydrogeochemical analysis of flow paths and
694 geochemical evolution in waters entering the basin and in the recharge areas to delineate flow
695 regimes in the groundwater system at much finer resolution and with depth; iii) paleo-hydrologic
696 reconstruction of conditions at the high elevation basins, groundwater discharge sites along the
697 margin of Salar de Atacama and within the evaporite depocenter; and iv) fully integrated
698 hydrogeological modeling to physically resolve the nature and time scales over which these
699 systemwide connections exist.

700 **7. Acknowledgments**

701 The authors want to thank Scott Hynek for the extensive advice and consultation he
702 provided on this work, it greatly improved the clarity of this manuscript; and Linda Godfrey for
703 providing valuable unpublished data to supplement our dataset. We would also like to
704 acknowledge Albemarle Corp. for their continued support of this and related research to improve
705 the fundamental understanding of the hydrogeology and geochemistry of the Salar de Atacama
706 environment. We are grateful for their permission to publish geochemical data relevant to this
707 manuscript. The ASTER DEM and Landsat 8 OLI were retrieved from EarthExplorer, courtesy of
708 the NASA Land Processes Distributed Active Archive Center, USGS/Earth Resources
709 Observation and Science Center. The data used in this work is available on the WaterIsotopes
710 Database (http://wateriso.utah.edu/waterisotopes/pages/spatial_db.html).

711 **Figure Captions:**

712 **Figure 1.** Digital elevation map of the Central Andes. Salars, lagoons and major drainages
713 (quebradas and rivers) are light blue. Topographic watersheds of major basins are outlined in
714 black. Extent of the Preandean Depression and Altiplano-Puna plateau are outlined in white
715 dashes. Isohyetal contours in mm/year are dark blue dashed lines. Locations of generalized
716 geologic cross-sections in Figure S1 are red. Red dots are precipitation gauges and sites used for
717 HYSPLIT models. MNT Trough structure is shaded.

718 **Figure 2.** The Salar de Atacama topographic watershed (solid black line), its recharge zones
719 (black dashed ellipses) and discharge/inflow zones (solid colored lines). Dots represent sample
720 sites, grouped by water type. Discharge zones extend from the salar margin to 4000 mamsl.
721 Major drainages (quebradas and rivers) are shown in white and salars and lagoons in light blue
722 and dark blue respectively. Notable high elevation lagoons Miñiques, Miscanti and Lejía are
723 labeled. Surface expression of the Peine/Cas structure is hatched.

724 **Figure 3.** Modern water content in samples (n=87) proportional to circle size. Shaded areas are
725 inflow water zones. Data from Grosjean et al. (1995) are orange. Circles in Nucleus and
726 Transition Zone represent averages of water bodies. Surface waters (sw) are outlined in red,
727 groundwaters (gw) in blue.

728 **Figure 4. (a)** Modern water proportion (R_{mod}) among groundwater and surface water bodies
729 along a transect of the eastern Salar de Atacama margin. South Inflow and East Inflow waters
730 are averaged as a single low elevation inflow water body. Mean R_{mod} value of each water
731 grouping (in black rectangles) and mean Specific Conductivity (SC) in mS/cm. **(b)** Tukey box plot
732 of 3H content (TU) in these water bodies. Blue dashed line is the theoretical maximum limit
733 (0.15TU) of background 3H produced in-situ by water-rock interaction.

734 **Figure 5.** $\delta^{18}O$ and δ^2H of water from the Salar de Atacama regional watershed (n=889). Colors
735 correspond to the three inflow zones labeled in Figure 2, brown points are all plateau waters.
736 The meteoric source water isotopic signature is estimated for each zone where the LEL
737 intersects the Local Meteoric Water line (LMWL) from Chaffaut et al. (1998). High-temperature
738 waters from the El Tatio thermal field and northern Puna region indicated by red Xs.

739 **Figure 6.** $\delta^{18}O$ and δ^2H of water from the plateau and divide recharge zones. Inflow waters (NE
740 and SE zones) are red and blue points displayed for context. Predicted meteoric source waters
741 from LEL intercept with LMWL are colored numbers.

742 **Figure 7.** $\delta^{18}O$ in waters from each zone plotted against sample elevation. Recharge limit line
743 denotes elevation below which no significant recharge occurs; Houston (2009), Scheihing et al.
744 (2018) and others have shown for this region the limit lies at ~120mm of precipitation per year
745 (Figure 1). Blue shaded envelope represents the salar evaporite aquifer below the basin floor.
746 Specific Conductivity ($\mu S/cm$) of sample groupings in italics. Ellipses in **(a)**, **(b)** and **(c)** indicate
747 descriptive groupings discussed in text and blue arrows indicate general hydrochemical
748 evolutionary pathways. Dashed arc in **(d)** indicates the predicted trend of isotopic evolution in a
749 river system. Water types and locations are labeled in legend (Spr.=Spring water).

750 **Figure 8.** Conceptual model of the Salar de Atacama regional groundwater system, major
751 mechanisms governing the contemporary hydrologic system and their relative influence

752 (adapted from Corenthal et al. 2016). In plan view **(a)**, solid light blue arrows represent the
753 distribution of modern meteoric inputs and their signatures, the brown dashed line denotes a
754 major orographic barrier to precipitation east of Miñiques and Miscanti lakes. Solid blue arrows
755 represent inflows of modern recharge, green dashed arrows are major inputs of paleo-
756 groundwater, red dashed arrows show hypothesized influx of solute-rich fluid. **(b)** Cross-
757 sectional view of the SE zone shows the distribution and relative importance of these
758 hydrological mechanisms. Blue lines are estimated position of the modern water table, green is
759 the LGM water table and the corresponding flow paths of modern and fossil groundwater, red is
760 solute-rich influx.

761 **Table Captions:**

762 **Table 1.** Calculations of transit time estimates assuming piston flow and a decay constant. The
763 High elevation lake water ^3H value and modern meteoric water are used as input ^3H values.
764 These input values were decayed and seepage velocities (v) estimated with aquifer properties (K
765 & θ) from Houston (2007) and a plausible range of values. Velocities were calculated by piston
766 flow transit times, then the MRT of waters were estimated under these conditions.

767

768 **References**

769

- 770 Allmendinger, R. W., Jordan, T. E., Kay, S. M., & Isacks, B. L. (1997). The Evolution of The
771 Altiplano-Puna Plateau of the Central Andes. *Annual Review of Earth and Planetary*
772 *Sciences*, 25(1), 139–174. <https://doi.org/10.1146/annurev.earth.25.1.139>
- 773 Ammann, C., Jenny, B., Kammer, K., & Messerli, B. (2001). Late quaternary glacier response to
774 humidity changes in the arid Andes of Chile (18-29°S). *Palaeogeography,*
775 *Palaeoclimatology, Palaeoecology*, 172(3–4), 313–326. [https://doi.org/10.1016/S0031-](https://doi.org/10.1016/S0031-0182(01)00306-6)
776 [0182\(01\)00306-6](https://doi.org/10.1016/S0031-0182(01)00306-6)
- 777 Aravena, R. (1995). Isotope hydrology and geochemistry of northern Chile groundwaters.
778 *Bulletin - Institut Francais d'Etudes Andines*, 24(3), 495–503.
- 779 Aravena, R., Suzuki, O., Peña, H., Pollastri, a., Fuenzalida, H., & Grilli, a. (1999). Isotopic
780 composition and origin of the precipitation in Northern Chile. *Applied Geochemistry*,
781 14(4), 411–422. [https://doi.org/10.1016/S0883-2927\(98\)00067-5](https://doi.org/10.1016/S0883-2927(98)00067-5)
- 782 Aron, F., González, G., Veloso, E., & Cembrano, J. (2008). Architecture and style of compressive
783 Neogene deformation in the eastern-southeastern border of the Salar de Atacama Basin
784 (22 30'-24 15'S): A structural setting for the active volcanic arc of the Central Andes. In
785 7th International Symposium on Andean Geodynamics (ISAG 2008, Nice) (pp. 52-55)
- 786 Barnes, C. J., & Allison, G. B. (1988). Tracing of water movement in the unsaturated zone using
787 stable isotopes of hydrogen and oxygen. *Journal of Hydrology*, 100(1–3), 143–176.
788 [https://doi.org/10.1016/0022-1694\(88\)90184-9](https://doi.org/10.1016/0022-1694(88)90184-9)
- 789 Barnes, C. J., & Walker, G. R. (1989). The distribution of deuterium and oxygen-18 during
790 unsteady evaporation from a dry soil. *Journal of Hydrology*, 112(1–2), 55–67.
791 [https://doi.org/10.1016/0022-1694\(89\)90180-7](https://doi.org/10.1016/0022-1694(89)90180-7)
- 792 Belcher, W. R., Bedinger, M. S., Back, J. T., & Sweetkind, D. S. (2009). Interbasin flow in the
793 Great Basin with special reference to the southern Funeral Mountains and the source of
794 Furnace Creek springs, Death Valley, California, U.S. *Journal of Hydrology*, 369(1–2),
795 30–43. <https://doi.org/10.1016/j.jhydrol.2009.02.048>
- 796 Bershaw, J., S. M. Penny, and C. N. Garzzone (2012). Stable isotopes of modern water across the
797 Himalaya and eastern Tibetan Plateau: Implications for estimates of paleoelevation and
798 paleoclimate, *J. Geophysical. Research*, 117, D02110, doi:10.1029/2011JD016132

- 799 Betancourt, J. L., Latorre, C., Rech, J. A., Quade, J., & Rylander, K. A. (2000). A 22,000-year
800 record of monsoonal precipitation from northern Chile's Atacama Desert. *Science*,
801 289(5484), 1542-1546
- 802 Beria, H., Larsen, J. R., Ceperley, N. C., Michelon, A., Vennemann, T., & Schaeffli, B. (2018).
803 Understanding snow hydrological processes through the lens of stable water isotopes.
804 *Wiley Interdisciplinary Reviews: Water*, 5(6), e1311. <https://doi.org/10.1002/wat2.1311>
- 805 Blard, P. H., Sylvestre, F., Tripathi, A. K., Claude, C., Causse, C., Coudrain, A., ... Lavé, J.
806 (2011). Lake highstands on the Altiplano (Tropical Andes) contemporaneous with
807 Heinrich 1 and the Younger Dryas: New insights from ^{14}C , U-Th dating and $\delta^{18}\text{O}$ of
808 carbonates. *Quaternary Science Reviews*, 30(27–28), 3973–3989.
809 <https://doi.org/10.1016/j.quascirev.2011.11.001>
- 810 Blodgett, T. a., J. D. Lenters, and B. L. Isacks (1997). Constraints on the origin of paleolake
811 expansions in the Central Andes, *Earth Interact.*, 1(1), 1–1, doi:10.1175/1087-
812 3562(1997)001<0001: CotOoP>2.0.CO;2
- 813 Bobst, A. L., Lowenstein, T. K., Jordan, T. E., Godfrey, L. V., Ku, T. L., & Luo, S. (2001). A 106
814 ka paleoclimate record from drill core of the Salar de Atacama, northern Chile.
815 *Palaeogeography, Palaeoclimatology, Palaeoecology*, 173(1–2), 21–42.
816 [https://doi.org/10.1016/S0031-0182\(01\)00308-X](https://doi.org/10.1016/S0031-0182(01)00308-X)
- 817 Boers, N., Bookhagen, B., Marwan, N., & Kurths, J. (2016). Spatiotemporal characteristics and
818 synchronization of extreme rainfall in South America with focus on the Andes Mountain
819 range. *Climate dynamics*, 46(1-2), 601-617
- 820 Boschetti, T., Cortecci, G., Barbieri, M., & Mussi, M. (2007). New and past geochemical data on
821 fresh to brine waters of the Salar de Atacama and Andean Altiplano, northern Chile.
822 *Geofluids*, 7(1), 33-50.
- 823 Boschetti, Cifuentes, Iacumin, & Selmo. (2019). Local Meteoric Water Line of Northern Chile
824 (18°S – 30°S): An Application of Error-in-Variables Regression to the Oxygen and
825 Hydrogen Stable Isotope Ratio of Precipitation. *Water*, 11(4), 791.
826 doi:10.3390/w11040791
- 827 Boutt, D. F., Hynek, S. A., Munk, L. A., & Corenthal, L. G. (2016). Rapid recharge of fresh water
828 to the halite-hosted brine aquifer of Salar de Atacama, Chile. *Hydrological Processes*,
829 30(25), 4720–4740. <https://doi.org/10.1002/hyp.10994>
- 830 Boutt, D., Corenthal, L., Munk, L. A., & Hynek, S. (2018). Imbalance in the modern hydrologic
831 budget of topographic catchments along the western slope of the Andes (21 – 25°S).
832 <https://doi.org/10.31223/osf.io/p5tsq>
- 833 Breitkreuz, C. (1995). The late Permian Peine and Cas Formations at the eastern margin of the
834 Salar de Atacama, Northern Chile: stratigraphy, volcanic facies, and tectonics. *Revista*
835 *Geológica de Chile*, 22(1), 3–23.
- 836 Burg, A., Zilberbrand, M., & Yechieli, Y. (2013). Radiocarbon Variability in Groundwater in an
837 Extremely Arid Zone—The Arava Valley, Israel. *Radiocarbon*, 55(2), 963–978.
838 <https://doi.org/10.1017/s0033822200058112>
- 839 Cartwright, I., Cendón, D., Currell, M., & Meredith, K. (2017). A review of radioactive isotopes
840 and other residence time tracers in understanding groundwater recharge: Possibilities,
841 challenges, and limitations. *Journal of Hydrology*, 555, 797–811.
842 <https://doi.org/10.1016/j.jhydrol.2017.10.053>
- 843 Cervetto Sepúlveda, M. M. (2012). Caracterización hidrogeológica e hidrogeoquímica de las
844 cuencas: Salar de Aguas calientes 2, Puntas negras, Laguna Tuyajto, Pampa Colorada,
845 Pampa Las Tecas y Salar el Laco, II región de Chile.
- 846 Chaffaut I, Coudrain-Ribstein A, Michelot JL, Pouyaud B. (1998) Precipitations d'altitude du
847 Nord-Chili, origine des sources de vapeur et donnees isotopiques. *Bulletin de l'Institute*
848 *Francais d etudes andine*, 27, 367–84.

- 849 Clark, I. D. 1., & Fritz, P. 1. (1997). Environmental isotopes in hydrogeology. Boca Raton, FL:
850 CRC Press/Lewis Publishers.
- 851 Clarke, W.B., Jenkins, W.J., Top, Z. (1976). Determination of Tritium by Mass Spectrometric
852 Measurement of ^3He . *International Journal of Applied Radiation and Isotopes* 27, 515–
853 522.
- 854 Cook PG, Bohlke J-K. (2000). Determining timescales for groundwater flow and solute transport.
855 In *Environmental Tracers in Subsurface Hydrology*, Cook PG, Herczeg AL (eds). Kluwer
856 Academic Publishers: Norwell, MA; 1–30.
- 857 Corenthal, L. G., Boutt, D. F., Hynek, S. A., & Munk, L. A. (2016). Regional groundwater flow
858 and accumulation of a massive evaporite deposit at the margin of the Chilean Altiplano.
859 *Geophysical Research Letters*, 43(15), 8017–8025. <https://doi.org/10.1002/2016GL070076>
- 860 Cortecchi, G., Boschetti, T., Mussi, M., Lameli, C. H., Mucchino, C., & Barbieri, M. (2005). New
861 chemical and original isotopic data on waters from El Tatio geothermal field, northern
862 Chile. *Geochemical Journal*, 39(6), 547–571. <https://doi.org/10.2343/geochemj.39.547>
- 863 Currell, M., Gleeson, T., Dahlhaus, P. (2016). A New Assessment Framework for Transience in
864 Hydrogeological Systems. *Groundwater* 54, 4–14. doi:10.1111/gwat.12300
- 865 DePaolo, D. J., M. E. Conrad, K. Maher, and G. W. Gee. 2004. Evaporation Effects on Oxygen
866 and Hydrogen Isotopes in Deep Vadose Zone Pore Fluids at Hanford, Washington.
867 *Vadose Zone J.* 3:220-232. doi:10.2136/vzj2004.2200
- 868 De Porras, M. E., Maldonado, A., De Pol-Holz, R., Latorre, C., & Betancourt, J. L. (2017). Late
869 Quaternary environmental dynamics in the Atacama Desert reconstructed from rodent
870 midden pollen records. *Journal of Quaternary Science*, 32(6), 665–684.
871 <https://doi.org/10.1002/jqs.2980>
- 872 DGA [Dirección General de Aguas] (2013), Análisis de la Oferta Hídrica del Salar de Atacama,
873 Santiago, Chile.
- 874 Draxler, R. R., & G. D. Hess (1998). An overview of the HYSPLIT_4 modelling system for
875 trajectories, dispersion and deposition, *Aust. Meteorol. Mag.*, 47(4), 295–308.
- 876 Eugster, H. P. (1980). Geochemistry of evaporitic lacustrine deposits. *Annual Review of Earth*
877 *and Planetary Sciences: Volume 8*, 35–63.
- 878 Favreau, G., Cappelaere, B., Massuel, S., Leblanc, M., Boucher, M., Boulain, N., & Leduc, C.
879 (2009). Land clearing, climate variability, and water resources increase in semiarid
880 southwest Niger: A review. *Water Resources Research*, 45(7).
881 <https://doi.org/10.1029/2007WR006785>
- 882 Fiorella, R. P., Poulsen, C. J., Pillco Zolá, R. S., Barnes, J. B., Tabor, C. R., & Ehlers, T. A.
883 (2015). Spatiotemporal variability of modern precipitation $\delta^{18}\text{O}$ in the central Andes and
884 implications for paleoclimate and paleoaltimetry estimates. *Journal of Geophysical*
885 *Research*, 120(10), 4630–4656. <https://doi.org/10.1002/2014JD022893>
- 886 Fontes, J C, & Molinari, J. (1975). Isotopic study of the upper watershed of the Rio Abancan
887 (Province of Catamarca, Argentina). *Rev. Geogr. Phys. Geol. Dyn.; (France); Journal*
888 *Volume: 7:5*
- 889 Fritz, P., Silva, H., Suzuki, O., & Salati, E. (1979). Isotope hydrology in northern Chile. In
890 *Isotope hydrology 1978*.
- 891 Fritz, P., Suzuki, O., Silva, C., & Salati, E. (1981). Isotope hydrology of groundwaters in the
892 Pampa del Tamarugal, Chile. *Journal of Hydrology*, 53(1–2), 161–184.
893 [https://doi.org/10.1016/0022-1694\(81\)90043-3](https://doi.org/10.1016/0022-1694(81)90043-3)
- 894 Fritz, S. C., P. a. Baker, T. K. Lowenstein, G. O. Seltzer, C. a. Rigsby, G. S. Dwyer, P. M. Tapia,
895 K. K. Arnold, T. L. Ku, and S. Luo (2004). Hydrologic variation during the last 170,000
896 years in the southern hemisphere tropics of South America, *Quat. Res.*, 61(1), 95–104.
897 doi: 10.1016/j.yqres.2003.08.007

- 898 Gardeweg, M., & Ramírez, C. F. (1987). La Pacana caldera and the Atana Ignimbrite - a major
899 ash-flow and resurgent caldera complex in the Andes of northern Chile. *Bulletin of*
900 *Volcanology*, 49(3), 547–566. <https://doi.org/10.1007/BF01080449>
- 901 Garreaud, R., M. Vuille, & A. C. Clement (2003). The climate of the Altiplano: Observed current
902 conditions and mechanisms of past changes, *Palaeogeography, Palaeoclimatology,*
903 *Palaeoecology.*, 194(1-3), 5–22, doi:10.1016/S0031-0182(03)00269-4.
- 904 Garreaud, R. D. (2009). The Andes climate and weather. *Advances in Geosciences*, 22, 3–11.
905 <https://doi.org/10.5194/adgeo-22-3-2009>
- 906 Gasse, F. (2000). Hydrological changes in the African tropics since the Last Glacial Maximum. In
907 *Quaternary Science Reviews* (Vol. 19, pp. 189–211). [https://doi.org/10.1016/S0277-](https://doi.org/10.1016/S0277-3791(99)00061-X)
908 [3791\(99\)00061-X](https://doi.org/10.1016/S0277-3791(99)00061-X)
- 909 Ge, J., Chen, J., Ge, L., Wang, T., Wang, C., & Chen, Y. (2016). Isotopic and hydrochemical
910 evidence of groundwater recharge in the Hopq Desert, NW China. *Journal of*
911 *Radioanalytical and Nuclear Chemistry*, 310(2), 761–775. [https://doi.org/10.1007/s10967-](https://doi.org/10.1007/s10967-016-4856-8)
912 [016-4856-8](https://doi.org/10.1007/s10967-016-4856-8)
- 913 Gleeson, T., L. Marklund, L. Smith, and A. H. Manning (2011), Classifying the water table at
914 regional to continental scales, *Geophys. Res. Lett.*, 38, L05401, doi:10.1029/
915 [2010GL046427](https://doi.org/10.1029/2010GL046427).
- 916 Gleeson, T., Wada, Y., Bierkens, M.F.P., van Beek, L.P.H., (2012). Water balance of global
917 aquifers revealed by groundwater footprint. *Nature* 488, 197–200.
918 doi:10.1038/nature11295
- 919 Godfrey, L. V., Jordan, T. E., Lowenstein, T. K., & Alonso, R. L. (2003). Stable isotope
920 constraints on the transport of water to the Andes between 22° and 26°S during the last
921 glacial cycle. In *Palaeogeography, Palaeoclimatology, Palaeoecology* (Vol. 194, pp. 299–
922 317). Elsevier B.V. [https://doi.org/10.1016/S0031-0182\(03\)00283-9](https://doi.org/10.1016/S0031-0182(03)00283-9)
- 923 González, G., Cembrano, J., Aron, F., Veloso, E. E., & Shyu, J. B. H. (2009). Coeval
924 compressional deformation and volcanism in the central Andes, case studies from northern
925 Chile (23°S–24°S). *Tectonics*, 28(6). <https://doi.org/10.1029/2009TC002538>
- 926 Grosjean, M., Geyh, M. A., Messerli, B., & Schotterer, U. (1995). Late-glacial and early
927 Holocene lake sediments, ground-water formation and climate in the Atacama Altiplano
928 22–24°S. *Journal of Paleolimnology*, 14(3), 241–252.
929 <https://doi.org/10.1007/BF00682426>.
- 930 Hartley, A. J., and G. Chong (2002), Late Pliocene age for the Atacama Desert: Implications for
931 the desertification of western South America, *Geology*, 30(1), 43–46, doi:10.1130/0091-
932 [7613\(2002\)030<0043: LPAFTA>2.0.CO;2](https://doi.org/10.1130/0091-7613(2002)030<0043: LPAFTA>2.0.CO;2)
- 933 Haitjema, H. M., & S. Mitchell-Bruker (2005), Are water tables a subdued replica of the
934 topography? *Ground Water*, 43, 781–786.
- 935 Herrera, C., Custodio, E., Chong, G., Lambán, L. J., Riquelme, R., Wilke, H., ... Lictevout, E.
936 (2016). Groundwater flow in a closed basin with a saline shallow lake in a volcanic area:
937 Laguna Tuyajto, northern Chilean Altiplano of the Andes. *Science of the Total*
938 *Environment*, 541, 303–318. <https://doi.org/10.1016/j.scitotenv.2015.09.060>
- 939 Houston, J. (2002). Groundwater recharge through an alluvial fan in the Atacama Desert,
940 northern Chile: mechanisms, magnitudes and causes. *Hydrological processes*, 16(15),
941 3019–3035.
- 942 Houston, J. (2006a). The great Atacama flood of 2001 and its implications for Andean hydrology.
943 *Hydrological Processes*, 20(3), 591–610. <https://doi.org/10.1002/hyp.5926>
- 944 Houston, J. (2006b). Variability of precipitation in the Atacama Desert: its causes and
945 hydrological impact. *International Journal of Climatology*, 26(15), 2181–2198.
- 946 Houston, J. (2007). Recharge to groundwater in the Turi Basin, northern Chile: An evaluation
947 based on tritium and chloride mass balance techniques. *Journal of Hydrology*, 334(3–4),
948 534–544. <https://doi.org/10.1016/j.jhydrol.2006.10.030>

- 949 Houston, J. (2009). A recharge model for high altitude, arid, Andean aquifers. *Hydrological*
950 *Processes*, 23(16), 2383–2393. <https://doi.org/10.1002/hyp.7350>
- 951 Houston, J. & Hart, D. (2004). Theoretical head decay in closed basin aquifers: an insight into
952 fossil groundwater and recharge events in the Andes of northern Chile. *Quarterly Journal*
953 *of Engineering Geology and Hydrogeology* 37, 131–139. doi:10.1144/1470-9236/04-007
- 954 Jasechko, S. (2016). Partitioning young and old groundwater with geochemical tracers. *Chemical*
955 *Geology*, 427, 35–42. <https://doi.org/10.1016/j.chemgeo.2016.02.012>
- 956 Jasechko, S., S. J. Birks, T. Gleeson, Y. Wada, P. J. Fawcett, Z. D. Sharp, J. J. McDonnell, and J.
957 M. Welker (2014). The pronounced seasonality of global groundwater recharge, *Water*
958 *Resour. Res.*, 50, 8845–8867, doi:10.1002/2014WR015809
- 959 Jasechko, S., Perrone, D., Befus, K. M., Bayani Cardenas, M., Ferguson, G., Gleeson, T., ...
960 Kirchner, J. W. (2017). Global aquifers dominated by fossil groundwaters but wells
961 vulnerable to modern contamination. *Nature Geoscience*, 10(6), 425–429.
962 <https://doi.org/10.1038/ngeo2943>
- 963 Jordan, T. E., L. V. Godfrey, N. Munoz, R. N. Alonso, T. K. Lowenstein, G. D. Hoke, N.
964 Peranginangin, B. L. Isacks, and L. Cathles (2002), *Orogenic-scale ground water*
965 *circulation in the Central Andes: evidence and consequences.*, 5th ISAG (International
966 *Symp. Andean Geodyn.*, 331–334.
- 967 Jordan, T. E., Nester, P. L., Blanco, N., Hoke, G. D., Dávila, F., & Tomlinson, A. J. (2010).
968 Uplift of the Altiplano-Puna plateau: A view from the west. *Tectonics*, 29(5).
969 <https://doi.org/10.1029/2010TC002661>
- 970 Jordan, T., Lameli, C. H., Kirk-Lawlor, N., & Godfrey, L. (2015). Architecture of the aquifers of
971 the Calama Basin, Loa catchment basin, northern Chile. *Geosphere*, 11(5), 1438–1474.
972 <https://doi.org/10.1130/GES01176.1>
- 973 Jordan, T. E., Herrera L., C., Godfrey, L. V., Colucci, S. J., Gamboa P., C., Urrutia M., J., ...
974 Paul, J. F. (2019). Isotopic characteristics and paleoclimate implications of the extreme
975 precipitation event of march 2015 in Northern Chile. *Andean Geology*, 46(1), 1–31.
976 <https://doi.org/10.5027/andgeov46n1-3087>
- 977 Kafri, U., & Yechieli, Y. (2012). The relationship between current and paleo groundwater base-
978 levels. *Quaternary International*, 257, 83–96. <https://doi.org/10.1016/j.quaint.2011.08.028>
- 979 Kampf, S. K., & Tyler, S. W. (2006). Spatial characterization of land surface energy fluxes and
980 uncertainty estimation at the Salar de Atacama, Northern Chile. *Advances in Water*
981 *Resources*, 29(2), 336–354. <https://doi.org/10.1016/j.advwatres.2005.02.017>
- 982 Kendall, C., & Caldwell, E. A. (1998). *Fundamentals of Isotope Geochemistry*. In *Isotope Tracers*
983 *in Catchment Hydrology* (pp. 51–86). Elsevier. [https://doi.org/10.1016/b978-0-444-](https://doi.org/10.1016/b978-0-444-81546-0.50009-4)
984 [81546-0.50009-4](https://doi.org/10.1016/b978-0-444-81546-0.50009-4)
- 985 Kendall, C., & McDonnell, J. J. (1998). *Isotope tracers in catchment hydrology*. *Isotope tracers in*
986 *catchment hydrology*. Elsevier Science B.V.
- 987 Kirchner, J. W. (2006). Getting the right answers for the right reasons: Linking measurements,
988 analyses, and models to advance the science of hydrology. *Water Resources Research*,
989 42(3). <https://doi.org/10.1029/2005WR004362>
- 990 Koeniger, P., Gaj, M., Beyrer, M., & Himmelsbach, T. (2016). Review on soil water isotope-based
991 groundwater recharge estimations. *Hydrological Processes*, 30(16), 2817–2834.
992 <https://doi.org/10.1002/hyp.10775>
- 993 Kröpelin, S., Verschuren, D., Lézine, A. M., Eggermont, H., Cocquyt, C., Francus, P., ...
994 Engstrom, D. R. (2008). Climate-driven ecosystem succession in the Sahara: The past
995 6000 years. *Science*, 320(5877), 765–768. <https://doi.org/10.1126/science.1154913>
- 996 Langenbrunner, B., Pritchard, M. S., Kooperman, G. J., & Randerson, J. T. (2019). Why Does
997 Amazon Precipitation Decrease When Tropical Forests Respond to Increasing CO₂?
998 *Earth's Future*, 7(4), 450–468. <https://doi.org/10.1029/2018EF001026>

- 999 Landwehr, J. M., & Coplen, T. B. (2006). Line-conditioned excess: a new method for
1000 characterizing stable hydrogen and oxygen isotope ratios in hydrologic systems.
1001 International conference on isotopes in environmental studies (pp. 132–135).
- 1002 Latorre, C., Betancourt, J. L., Rylander, K. A., Quade, J., & Matthei, O. (2003). A vegetation
1003 history from the arid prepuna of northern Chile (22–23°S) over the last 13 500 years. In
1004 Palaeogeography, Palaeoclimatology, Palaeoecology (Vol. 194, pp. 223–246). Elsevier
1005 B.V. [https://doi.org/10.1016/S0031-0182\(03\)00279-7](https://doi.org/10.1016/S0031-0182(03)00279-7)
- 1006 Lindsey, B.D., Jurgens, B.C., and Belitz, K. (2019). Tritium as an indicator of modern, mixed,
1007 and premodern groundwater age: U.S. Geological Survey Scientific Investigations Report
1008 2019–5090, 18 p., <https://doi.org/10.3133/sir20195090>
- 1009 Love, A. H., & Zdon, A. (2018). Use of radiocarbon ages to narrow groundwater recharge
1010 estimates in the southeastern Mojave Desert, USA. *Hydrology*, 5(3).
1011 <https://doi.org/10.3390/hydrology5030051>
- 1012 Lowenstein, T. K., Hein, M. C., Bobst, A. L., Jordan, T. E., Ku, T.-L., & Luo, S. (2003). An
1013 Assessment of Stratigraphic Completeness in Climate-Sensitive Closed-Basin Lake
1014 Sediments: Salar de Atacama, Chile. *Journal of Sedimentary Research*, 73(1), 91–104.
1015 <https://doi.org/10.1306/061002730091>
- 1016 Lucas, L.L., Unterweger (2000). Comprehensive Review and Critical Evaluation of the Half-Life
1017 of Tritium. *Journal of Research of the National Institute of Standards and Technology* 105,
1018 541–549.
- 1019 Magaritz, M., Aravena, R., Peña, H., Suzuki, O., & Grilli, A. (1989). Water chemistry and isotope
1020 study of streams and springs in northern Chile. *Journal of Hydrology*, 108(C), 323–341.
1021 [https://doi.org/10.1016/0022-1694\(89\)90292-8](https://doi.org/10.1016/0022-1694(89)90292-8)
- 1022 Magilligan, F. J., Goldstein, P. S., Fisher, G. B., Bostick, B. C., & Manners, R. B. (2008). Late
1023 Quaternary hydroclimatology of a hyper-arid Andean watershed: Climate change, floods,
1024 and hydrologic responses to the El Niño-Southern Oscillation in the Atacama Desert.
1025 *Geomorphology*, 101(1–2), 14–32. <https://doi.org/10.1016/j.geomorph.2008.05.025>
- 1026 Mather, A. E., & Hartley, A. (2005). Flow events on a hyper-arid alluvial fan: Quebrada
1027 Tambores, Salar de Atacama, northern Chile. *Geological Society Special Publication*, 251,
1028 9–24. <https://doi.org/10.1144/GSL.SP.2005.251.01.02>
- 1029 Maxey, G. B. (1968). Hydrogeology of Desert Basins. *Groundwater*, 6(5), 10–22.
1030 <https://doi.org/10.1111/j.1745-6584.1968.tb01660.x>
- 1031 McKnight, Sarah, (2019). "The Climatic and Hydrostratigraphic Controls on Brine-to-Freshwater
1032 Interface Dynamics in Hyperarid Climates: A 2-D Parametric Groundwater Modeling
1033 Study". Masters Theses. 785. https://scholarworks.umass.edu/masters_theses_2/785
- 1034 Meijer, A. & Kwicklis, E. (2000). Geochemical and Isotopic Constraints on Ground-Water Flow
1035 Directions, Mixing and Recharge at Yucca Mountain, Nevada. United States.
1036 doi:10.2172/883407
- 1037 Müller, T., Osenbrück, K., Strauch, G., Pavetich, S., Al-Mashaikhi, K. S., Herb, C., ... Sanford,
1038 W. (2016). Use of multiple age tracers to estimate groundwater residence times and long-
1039 term recharge rates in arid southern Oman. *Applied Geochemistry*, 74, 67–83.
1040 <https://doi.org/10.1016/j.apgeochem.2016.08.012>
- 1041 Munk, L. A., Boutt, D. F., Hynek, S. A., & Moran, B. J. (2018). Hydrogeochemical fluxes and
1042 processes contributing to the formation of lithium-enriched brines in a hyper-arid
1043 continental basin. *Chemical Geology*, 493, 37–57.
1044 <https://doi.org/10.1016/j.chemgeo.2018.05.013>
- 1045 Ortiz, C., Aravena, R., Briones, E., Suárez, F., Tore, C., & Muñoz, J. F. (2014). Sources of
1046 surface water for the Soncor ecosystem, Salar de Atacama basin, northern Chile.
1047 *Hydrological Sciences Journal*, 59(2), 336-350.

- 1048 Pascale, S., Carvalho, L. M. V., Adams, D. K., Castro, C. L., & Cavalcanti, I. F. A. (2019).
1049 Current and Future Variations of the Monsoons of the Americas in a Warming Climate.
1050 Current Climate Change Reports. Springer. <https://doi.org/10.1007/s40641-019-00135-w>
1051 Peralta Arnold, Y., Cabassi, J., Tassi, F., Caffè, P. J., & Vaselli, O. (2017). Fluid geochemistry of
1052 a deep-seated geothermal resource in the Puna plateau (Jujuy Province, Argentina).
1053 Journal of Volcanology and Geothermal Research, 338, 121–134.
1054 <https://doi.org/10.1016/j.jvolgeores.2017.03.030>
1055 Pérez-Fodich, A., Reich, M., Álvarez, F., Snyder, G. T., Schoenberg, R., Vargas, G., ... & Fehn,
1056 U. (2014). Climate change and tectonic uplift triggered the formation of the Atacama
1057 Desert's giant nitrate deposits. *Geology*, 42(3), 251–254.
1058 Pingel, H., Alonso, R. N., Altenberger, U., Cottle, J., & Strecker, M. R. (2019). Miocene to
1059 Quaternary basin evolution at the southeastern Andean Plateau (Puna) margin (ca. 24°S
1060 lat, Northwestern Argentina). *Basin Research*, 31(4), 808–826.
1061 <https://doi.org/10.1111/bre.12346>
1062 Placzek, C., Quade, J., & Patchett, P. J. (2006). Geochronology and stratigraphy of late
1063 Pleistocene lake cycles on the southern Bolivian Altiplano: Implications for causes of
1064 tropical climate change. *Bulletin of the Geological Society of America*, 118(5–6), 515–
1065 532. <https://doi.org/10.1130/B25770.1>
1066 Placzek, C., Quade, J., Betancourt, J. L., Patchett, P. J., Rech, J. A., Latorre, C., ... English, N. B.
1067 (2009). CLIMATE IN THE DRY CENTRAL ANDES OVER GEOLOGIC,
1068 MILLENNIAL, AND INTERANNUAL TIMESCALES. *Annals of the Missouri*
1069 *Botanical Garden*, 96(3), 386–397. <https://doi.org/10.3417/2008019>
1070 Placzek, C. J., Quade, J., & Patchett, P. J. (2013). A 130ka reconstruction of rainfall on the
1071 Bolivian Altiplano. *Earth and Planetary Science Letters*, 363, 97–108.
1072 <https://doi.org/10.1016/j.epsl.2012.12.017>
1073 Quade, J., Rech, J. A., Betancourt, J. L., Latorre, C., Quade, B., Rylander, K. A., & Fisher, T.
1074 (2008). Paleowetlands and regional climate change in the central Atacama Desert,
1075 northern Chile. *Quaternary Research*, 69(3), 343–360.
1076 Ramirez, C., and M. Gardeweg (1982). Carta Geologica de Chile, escala 1:250000, Hoja
1077 Toconao, Region de Antofagasta, Chile No. 54, Santiago, Chile.
1078 Rech, J. A., Quade, J., & Betancourt, J. L. (2002). Late Quaternary paleohydrology of the central
1079 Atacama Desert (lat 22°–24°S), Chile. *Bulletin of the Geological Society of America*,
1080 114(3), 334–348. [https://doi.org/10.1130/0016-7606\(2002\)114<0334:LQPOTC>2.0.CO;2](https://doi.org/10.1130/0016-7606(2002)114<0334:LQPOTC>2.0.CO;2)
1081 Rech, J. A., Pigati, J. S., Quade, J., & Betancourt, J. L. (2003). Re-evaluation of mid-Holocene
1082 deposits at Quebrada Puripica, northern Chile. In *Paleogeography, Paleoclimatology,*
1083 *Paleoecology* (Vol. 194, pp. 207–222). [https://doi.org/10.1016/S0031-0182\(03\)00278-5](https://doi.org/10.1016/S0031-0182(03)00278-5)
1084 Rech, J. A., Currie, B. S., Jordan, T. E., Riquelme, R., Lehmann, S. B., Kirk-Lawlor, N. E., ...
1085 Gooley, J. T. (2019). Massive middle Miocene gypsic paleosols in the Atacama Desert and
1086 the formation of the Central Andean rain-shadow. *Earth and Planetary Science Letters*,
1087 506, 184–194. <https://doi.org/10.1016/j.epsl.2018.10.040>
1088 Reutter, K. J., Charrier, R., Götze, H. J., Schurr, B., Wigger, P., Scheuber, E., ... & Chong, G.
1089 (2006). The Salar de Atacama Basin: a subsiding block within the western edge of the
1090 Altiplano-Puna Plateau. In *the Andes* (pp. 303–325). Springer Berlin Heidelberg.
1091 Risacher, F., Alonso, H., Salazar, C. (1999). Geoquímica de aguas en cuencas cerradas: I, II y III
1092 Regiones—Chile. I. Ministerio de Obras Públicas, pp. 209.
1093 Risacher, F., Alonso, H., & Salazar, C. (2003). The origin of brines and salts in Chilean salars: a
1094 hydrochemical review. *Earth-Science Reviews*, 63(3), 249–293.
1095 Rissmann, C., Leybourne, M., Benn, C., & Christenson, B. (2015). The origin of solutes within
1096 the groundwaters of a high Andean aquifer. *Chemical Geology*, 396, 164–181.
1097 <https://doi.org/10.1016/j.chemgeo.2014.11.029>

- 1098 Rohrmann, A., Strecker, M. R., Bookhagen, B., Mulch, A., Sachse, D., Pingel, H., ... Montero,
 1099 C. (2014). Can stable isotopes ride out the storms? The role of convection for water
 1100 isotopes in models, records, and paleoaltimetry studies in the central Andes. *Earth and*
 1101 *Planetary Science Letters*, 407, 187–195. <https://doi.org/10.1016/j.epsl.2014.09.021>
 1102 Rosen, M. R. (1994). The importance of groundwater in playas: A review of playa classifications
 1103 and the sedimentology and hydrology of playas. *Special Paper of the Geological Society*
 1104 *of America*, 289, 1–18. <https://doi.org/10.1130/SPE289-p1>
 1105 Sáez, A., Godfrey, L. V., Herrera, C., Chong, G., & Pueyo, J. J. (2016). Timing of wet episodes
 1106 in Atacama Desert over the last 15 ka. *The Groundwater Discharge Deposits (GWD) from*
 1107 *Domeyko Range at 25°S. Quaternary Science Reviews*, 145, 82–93.
 1108 <https://doi.org/10.1016/j.quascirev.2016.05.036>
 1109 Scanlon, B. R., Keese, K. E., Flint, A. L., Flint, L. E., Gaye, C. B., Edmunds, W. M., & Simmers,
 1110 I. (2006). Global synthesis of groundwater recharge in semiarid and arid regions.
 1111 *Hydrological Processes*, 20(15), 3335–3370. <https://doi.org/10.1002/hyp.6335>
 1112 Scheihing, K. W., Moya, C. E., Struck, U., Lictevout, E., & Tröger, U. (2018). Reassessing
 1113 hydrological processes that control stable Isotope Tracers in groundwater of the Atacama
 1114 Desert (Northern Chile). *Hydrology*, 5(1). <https://doi.org/10.3390/hydrology5010003>
 1115 Skrzypek, G., Dogramaci, S., Rouillard, A., & Grierson, P. F. (2016). Groundwater seepage
 1116 controls salinity in a hydrologically terminal basin of semi-arid northwest Australia.
 1117 *Journal of Hydrology*, 542, 627–636. <https://doi.org/10.1016/j.jhydrol.2016.09.033>
 1118 Stewart, M. K., Morgenstern, U., Gusyev, M. A., & Małoszewski, P. (2017). Aggregation effects
 1119 on tritium-based mean transit times and young water fractions in spatially heterogeneous
 1120 catchments and groundwater systems. *Hydrology and Earth System Sciences*, 21(9),
 1121 4615–4627. <https://doi.org/10.5194/hess-21-4615-2017>
 1122 Stigter, E. E., Litt, M., Steiner, J. F., Bonekamp, P. N. J., Shea, J. M., Bierkens, M. F. P., &
 1123 Immerzeel, W. W. (2018). The Importance of Snow Sublimation on a Himalayan Glacier.
 1124 *Frontiers in Earth Science*, 6. <https://doi.org/10.3389/feart.2018.00108>
 1125 Strecker, M. R., Alonso, R. N., Bookhagen, B., Carrapa, B., Hilley, G. E., Sobel, E. R., & Trauth,
 1126 M. H. (2007). Tectonics and Climate of the Southern Central Andes. *Annual Review of*
 1127 *Earth and Planetary Sciences*, 35(1), 747–787.
 1128 <https://doi.org/10.1146/annurev.earth.35.031306.140158>
 1129 Tóth, J. (1963). A theoretical analysis of groundwater flow in small drainage basins. *Journal of*
 1130 *Geophysical Research*, 68(16), 4795–4812. <https://doi.org/10.1029/jz068i016p04795>
 1131 Tsujimura, M., Abe, Y., Tanaka, T., Shimada, J., Higuchi, S., Yamanaka, T., ... Oyunbaatar, D.
 1132 (2007). Stable isotopic and geochemical characteristics of groundwater in Kherlen River
 1133 basin, a semi-arid region in eastern Mongolia. *Journal of Hydrology*, 333(1), 47–57.
 1134 <https://doi.org/10.1016/j.jhydrol.2006.07.026>
 1135 Tyler, S.W., Kranz, S., Parlange, M.B., Albertson, J., Katul, G.G., Cochran, G.F., Lyles, B.A.,
 1136 Holder, G. (1997). Estimation of groundwater evaporation and salt flux from Owens Lake,
 1137 California, USA. *Journal Hydrology* 200, 110–135.
 1138 Walvoord, M. A., Plummer, M. A., Phillips, F. M., & Wolfsberg, A. V. (2002). Deep arid system
 1139 hydrodynamics I. Equilibrium states and response times in thick desert vadose zones.
 1140 *Water Resources Research*, 38(12), 44-1-44–15. <https://doi.org/10.1029/2001WR000824>
 1141 Ward, K. M., Zandt, G., Beck, S. L., Christensen, D. H., & McFarlin, H. (2014). Seismic imaging
 1142 of the magmatic underpinnings beneath the Altiplano-Puna volcanic complex from the
 1143 joint inversion of surface wave dispersion and receiver functions. *Earth and Planetary*
 1144 *Science Letters*, 404, 43–53. <https://doi.org/10.1016/j.epsl.2014.07.022>
 1145 Ward, D. J., Cesta, J. M., Galewsky, J., & Sagredo, E. (2015). Late Pleistocene glaciations of the
 1146 arid subtropical Andes and new results from the Chajnantor Plateau, northern Chile.
 1147 *Quaternary Science Reviews*, 128, 98–116.
 1148 <https://doi.org/10.1016/j.quascirev.2015.09.022>

- 1149 WMC [Water Management Consultants Ltda.] (2007). Analisis de la relacion entre las aguas
1150 subterranas del Proyecto Pampa Colorada, las vertientes y del margen este del Salar de
1151 Atacama y las Lagunas Miscanti y Minique, Informe III Final, Santiago, Chile.
- 1152 Wheater, H., Sorooshian, S., & Sharma, K. D. (2007). Hydrological modelling in arid and semi-
1153 arid areas. *Hydrological Modelling in Arid and Semi-Arid Areas* (Vol. 9780521869188,
1154 pp. 1–212). Cambridge University Press. <https://doi.org/10.1017/CBO9780511535734>
- 1155 Wilson, J. L., & Guan, H. (2013). Mountain-Block Hydrology and Mountain-Front Recharge. In
1156 *Groundwater Recharge in a Desert Environment: The Southwestern United States* (Vol. 9,
1157 pp. 113–137). American Geophysical Union. <https://doi.org/10.1029/009WSA08>
- 1158 Wood, C., Cook, P. G., & Harrington, G. A. (2015). Vertical carbon-14 profiles for resolving
1159 spatial variability in recharge in arid environments. *Journal of Hydrology*, 520, 134–142.
1160 <https://doi.org/10.1016/j.jhydrol.2014.11.044>
- 1161 Van Beek, L.P.H., Wada, Y., Bierkens, M.F.P. (2011). Global monthly water stress: 1. Water
1162 balance and water availability. *Water Resources Research* 47, W07517.
1163 doi:10.1029/2010wr009791
- 1164 Vuille, M., & Ammann, C. (1997). Regional Snowfall Patterns in the High, Arid Andes. In
1165 *Climatic Change at High Elevation Sites* (pp. 181–191). Dordrecht: Springer Netherlands.
1166 https://doi.org/10.1007/978-94-015-8905-5_10
- 1167 Zimmerman, U., D. Ehhalt, and K.O. Munnich. (1967). Soil water movement and
1168 evapotranspiration: Changes in the isotopic composition of the water. Paper presented at
1169 International Atomic Energy Agency Symposium on Isotopes in Hydrology. Int. Atomic
1170 Energy Agency, Vienna, Austria.